The ortholog of chloroquine resistance transporter (TgCRT) plays a key role in maintaining the integrity of the endolysosomal system in *Toxoplasma gondii* to facilitate host invasion

L. Brock Thornton[1], Paige Teehan[1#a], Katherine Floyd[1¶], Christian Cochrane[1¶], Amy Bergmann[1¶], and Zhicheng Dou[1*]

1. Department of Biological Sciences, Clemson University, Clemson, South Carolina, United States of America

[#a]Current Address: Department of Biochemistry and Molecular Biology, The Pennsylvania State University, Pennsylvania, United States of America

*Corresponding author

E-mail: zdou@clemson.edu (ZD)

[¶]These authors contributed equally to this work.

Short title: Dynamics of the digestive vacuole in *Toxoplasma gondii*

Abstract

Toxoplasma gondii, with the ability to use foodborne, zoonotic, and congenital routes of transmission, is an apicomplexan parasite that can cause severe infectious disease in the immunocompromised human population. The parasites harbor a lysosome-like digestive vacuole, termed Vacuolar Compartment/Plant-Like Vacuole (VAC/PLV), which plays an important role in maintaining the lytic cycle and virulence of *Toxoplasma* parasites. The VAC supplies proteolytic enzymes that are required to maturate the parasite's invasion effectors and digest autophagosomes and endocytosed host proteins. Our previous study identified a *Toxoplasma* ortholog of malarial chloroquine resistance transporter that localized in the VAC. Here, we genetically ablate *TgCRT* and reveal that the TgCRT plays a key role in maintaining the integrity of parasite's endolysosomal system by controlling the morphology of the VAC. The VAC dramatically increases in size by ~15-fold and co-localizes with its adjacent endosome-like compartment when TgCRT is absent. To reduce the aberrant swelling, the parasites decrease the transcript and protein levels of endolysosomal proteases in Δ*crt* parasites. One subtilisin protease residing within the endolysosomal system was significantly reduced at both the transcription and translation stages, which impairs the trimming of micronemal proteins on the surface of the parasites, thereby decreasing parasite invasion. Our study also showed that chemical and genetic inhibition of proteolysis within the VAC reduces its size and partially restores the endolysosomal system, as well as invasion and micronemal protein trimming. In summary, these findings reveal for the first time a native role of this CRT ortholog in controlling the size of the VAC and integrity of the endolysosomal system in *Toxoplasma* parasites to facilitate parasite invasion of host cells. These observations also indicate the function of TgCRT in mediating the transport of small solutes to regulate osmotic pressure within the VAC. Our findings will help expand understanding of CRT orthologs in other apicomplexan parasites.

Author Summary

Toxoplasma gondii is an obligate intracellular protozoan parasite that belongs to the phylum Apicomplexa and infects virtually all warm-blooded organisms. Approximately one-third of the human population is infected with *Toxoplasma*. The parasites invade host cells by using processed invasion effectors to disseminate infection. A lysosome-like digestive vacuole is involved in refining these invasion effectors to reach their final forms. One malarial chloroquine resistance transporter-like protein was found to span the membrane of the digestive vacuole in *Toxoplasma*. Although the mutated version of the malarial chloroquine resistance transporter has been shown to confer resistance of chloroquine treatment in malaria parasites, its native role in apicomplexan parasites remains unknown. In this study, we report that this transmembrane protein plays a key role in regulating the integrity of the digestive vacuole and its adjacent organelles in *Toxoplasma* parasites, further affecting proteolytic physiology within these organelles, the secretion of invasion effectors, and parasite invasion and virulence. To relieve osmotic stress caused by swelling within the digestive vacuole, the parasites take a strategy of repression of proteolytic activities within this organelle to decrease the accumulation of small solutes in the lumen. Our findings suggest a native function of this chloroquine resistance transporter ortholog in *Toxoplasma* parasites. Further understanding the molecular mechanism used by *Toxoplasma* to maintain a functional digestive vacuole could shed light on the identification of therapeutic targets for managing toxoplasmosis.

60 **Introduction**

61 *Toxoplasma gondii*, a protozoan pathogen, uses its polypeptide invasion factors to efficiently invade
62 host cells. These proteins are stored in two unique organelles in *Toxoplasma* parasites, termed the
63 microneme and rhoptry. The micronemal proteins need to undergo a series of proteolytic cleavages within
64 the parasite's endosomal system, followed by further intramembrane cleavage and trimming on the
65 parasite's cell membrane before secretion [1,2]. Therefore, proper maturation and secretion of micronemal
66 proteins are crucial for efficient invasion of parasites [3-5].

67 Micronemal protein maturation and secretion are regulated by several proteases. During intracellular
68 trafficking, the micronemal proteins are first cleaved by the aspartyl protease 3 (TgASP3) in a post-Golgi
69 compartment for removal of their propeptide [5]. A cathepsin L-like protease (TgCPL) was also shown to
70 process some micronemal proteins in the endosome-like compartment (ELC) of the parasites [4]. The
71 mature micronemal proteins pass through the microneme and are subjected to further intramembrane
72 cleavage and trimming on the parasite's surface. A plasma membrane-bound protease, rhomboid 4
73 (TgROM4), is a major protease required to process some micronemal proteins and release them from the
74 cell surface of the parasites, including micronemal protein 2 (TgMIC2) and apical membrane antigen
75 (TgAMA1) [6-9]. Subsequently, one subtilisin ortholog, TgSUB1, was shown to trim some micronemal
76 proteins into their final forms, such as TgMIC2 and TgMIC2-associated protein (TgM2AP) [3]. Therefore,
77 the precise control of proteolytic activities within the parasite's endosomal system and on the cell
78 membrane is critical for the processing of parasite's invasion effectors and invasion.

79 Among these proteases, TgCPL and TgSUB1 are both localized in the parasite's endolysosomal
80 system. TgCPL is located in an acidic digestive vacuole, termed the Vacuolar Compartment/Plant-like
81 Vacuole (VAC/PLV, VAC hereafter for convenience) in *Toxoplasma* parasites [4,10]. Our previous studies
82 showed that the genetic ablation of *TgCPL* causes defects in parasite invasion and acute virulence [4,11].
83 TgCPL becomes activated in the VAC, and a portion of TgCPL is delivered to the juxtaposed ELC for
84 maturation of some micronemal proteins [4]. TgSUB1 is a micronemal protease and contains a GPI anchor
85 to help it stay on the surface of the cell membrane of parasites [3]. TgSUB1 was shown to be activated in
86 a post-ER compartment and enter the parasite's endolysosomal system before arrival to microneme [12].

87 The deletion of *TgSUB1* led to inefficient trimming of micronemal proteins on the parasite's surface, thereby
88 leading to invasion and virulence defects [3]. Hence, the maintenance of the integrity of the parasites'
89 endolysosomal system is critical for regulating the distribution and activity of endolysosomal proteases.

90 The VAC is an important organelle in the parasite's endolysosomal system. A dysfunctional VAC
91 results in the reduced invasion, replication, and virulence in acute infection of *Toxoplasma* [4,11]. Moreover,
92 the parasites are unable to turn over autophagosomes during chronic infection to sustain their survival in
93 the host's brain [13]. Despite its importance, the VAC has not been well characterized. Only 4 proteins
94 have been localized in the VAC, including TgCPL, TgCPB (a cathepsin B-like protein), TgCRT (a
95 *Toxoplasma* ortholog of chloroquine resistance transporter), and TgVP1 (a pyrophosphatase) [4,14-16].
96 The VAC forms an intact organelle during the initial infection and fragments throughout subsequent
97 intracellular replication [4]. It is still unknown how the parasites regulate the morphological changes of their
98 endolysosomal system. In a previous study, the *TgCRT* was knocked down in type I *Toxoplasma* parasites
99 using a tetracycline-inducible system [15], and it was observed that the VAC becomes swollen when
100 TgCRT is absent. Furthermore, the mutant parasites display fitness defects when TgCRT is repressed.
101 These findings indicate that the TgCRT is involved in controlling the morphology of the VAC.

102 Interestingly, the swollen phenotype of the TgCRT-deficient VAC mirrors the enlarged digestive
103 vacuole in chloroquine-resistant *Plasmodium falciparum*. An *in vitro* assay utilizing recombinant
104 *Plasmodium* CRT ortholog (PfCRT), reconstituted in proteoliposomes showed that the recombinant PfCRT
105 transports basic amino acids, synthesized hemoglobin-derived oligopeptides, and small drug molecules,
106 at the expense of a proton gradient potential [17]. It was also documented that the $PfCRT^{3D7}$ derived from
107 a chloroquine (CQ)-sensitive strain exhibits better transport efficiency than $PfCRT^{Dd2}$ and $PfCRT^{7G8}$ derived
108 from the CQ-resistant malaria strains. These findings suggest that the PfCRT could regulate the transport
109 of small solutes from the digestive vacuole to control its size and morphology. However, the inability to
110 successfully ablate the *PfCRT* gene in *Plasmodium* limits the understanding of its native function *in vivo*.

111 Here, we successfully delete the *TgCRT* gene in a Type I *Toxoplasma* parasite strain by double
112 crossover homologous recombination. The resulting mutant, Δ*crt,* displayed a swollen digestive vacuole,
113 which overlaps with the neighboring ELC. This aberrant organelle organization led to the reduction of

114 transcript and protein levels of several proteases residing in the parasite's endolysosomal system, further
115 altering microneme secretion and resulting in defective parasite invasion and acute virulence. Collectively,
116 these findings determine a novel role of TgCRT in regulating the size of the digestive vacuole to maintain
117 the integrity of the parasite's endolysosomal system in *Toxoplasma* parasites. Our results may also lead
118 to a better understanding of the functions of CRT orthologs in other apicomplexan parasites.
119

120 **Results**

121 **1. The *TgCRT* is genetically ablated in *Toxoplasma gondii*.**

122 *TgCRT* gene was documented to be refractory for genetic disruption and conditionally knocked down
123 by using an anhydrotetracycline-regulated system in a Type I *Toxoplasma* RH strain [15]. The resulting
124 inducible *TgCRT* knockdown parasites showed enlarged VAC and fitness defects when the transcription
125 of *TgCRT* is repressed [15]. However, the incomplete depletion of *TgCRT* limits the further characterization
126 of its role in the parasites. Here, we adopted a genetically tractable RH-derived strain, termed RH∆*ku80*
127 (hereafter referred to as WT), to produce a complete knockout of *TgCRT*. The RH∆*ku80* strain represses
128 the non-homologous end-joining DNA repair pathway to facilitate homology dependent DNA recombination
129 [18]. Due to its increased efficiency of DNA homologous recombination, this strain has been widely used
130 as a wild type strain in the *Toxoplasma* research field. We PCR amplified both the 5'- and 3'-untranslated
131 regions (UTRs) (~1.5kb each) of the *TgCRT* gene, and flanked both at the 5'- and 3'-ends of a bleomycin
132 (*BLE*) resistance cassette to assemble a *TgCRT* knockout plasmid. The resulting construct was transfected
133 into WT parasites to replace the entire *TgCRT* gene with a *BLE* resistance cassette by double crossover
134 homologous recombination (**Fig 1A**). To confirm the proper integration, PCR analysis was performed to
135 detect the presence of the *BLE* cassette and the loss of *TgCRT* gene by using the primers shown in the
136 schematic for the generation of the *TgCRT* knockout in Fig 1A. Amplification of ~1.6 kb fragments at both
137 the 5'- and 3'-end integration regions (5'- and 3'-ARMs) were observed in the *TgCRT*-deletion mutant (∆*crt*),
138 and a ~1.5 kb *TgCRT* coding region was missing in the ∆*crt* strain (**Fig 1B**).

139 To complement the ∆*crt* parasites, we modified the pTub-TgCRT-mCherry-3xmyc plasmid (a gift from
140 Dr. G. van Dooren, Australian National Laboratory), which over-expresses an mCherry-3xmyc epitope-

141 tagged *TgCRT* under the *Toxoplasma* tubulin promoter. A 1 kb DNA region containing the cognate
142 promoter of the *TgCRT* gene was PCR-amplified and used to replace the tubulin promoter by molecular
143 cloning to keep the transcription level of the complemented *TgCRT* the same as the endogenous *TgCRT*.
144 The same pair of primers that were used to detect the loss of *TgCRT* in the Δ*crt* strain in Fig 1B were used
145 to confirm the integration of the exogenously introduced *TgCRT* gene. Since the complemented *TgCRT*
146 gene lacks introns, a ~0.2 kb PCR product was observed in the Δ*crtCRT* complementation strain, whereas
147 a ~1.5 kb fragment was yielded in the WT strain (**Fig 1C**). To confirm that the transcript levels of *TgCRT*
148 in the Δ*crtCRT* strain were comparable to the levels in WT parasites, a SYBR® Green-based quantitative
149 PCR (qPCR) was used to quantify messenger RNA of *TgCRT* in WT, Δ*crt*, and Δ*crtCRT* strains. No *TgCRT*
150 transcripts were observed in Δ*crt*, further validating the successful gene disruption in the Δ*crt* mutant. The
151 transcript levels of *TgCRT* were similar between the WT and Δ*crtCRT* strains (**Fig 1D**). Collectively, we
152 successfully ablated the *TgCRT* gene in *Toxoplasma* parasites, and properly restored the expression of
153 the exogenously introduced *TgCRT* in the Δ*crtCRT* complementation strain in order to analyze the role of
154 TgCRT in *Toxoplasma* parasites.

155 **2. The TgCRT-deficient parasites lose the integrity of their endolysosomal system by altering the**
156 **morphology of the VAC.**

157 After obtaining the Δ*crt* mutant, we observed that purified extracellular Δ*crt* parasites exhibited large
158 concave subcellular structures under differential interference contrast (DIC) microscopy, whereas WT and
159 Δ*crtCRT* strains did not display this striking phenotype (**Fig 1E**). This enlarged subcellular structure was
160 also observed in Δ*crt* parasites during pulse invasion (**Fig 1F**). To identify the swollen structure as the VAC,
161 we stained the WT, Δ*crt*, and Δ*crtCRT* parasites with anti-TgCPL antibodies. TgCPL is a major luminal
162 endoprotease in the VAC of *Toxoplasma* [4,19]. Immunofluorescence microscopy showed that the TgCPL
163 staining nicely co-localized with the concave subcellular structure in the Δ*crt* mutant **(Fig 1F)**. The TgCPL
164 staining in the Δ*crt* mutant was bigger than that in WT and Δ*crtCRT* parasites, indicating that the VAC
165 becomes swollen when TgCRT is absent. We also quantified the sizes of the VACs based on the TgCPL
166 staining as described previously [13,15]. The diameter of the VAC in the Δ*crt* parasites (1.12 ± 0.07 μm,
167 mean ± standard deviation) is approximately 2.6-fold larger than that in WT parasites (0.43 ± 0.03 μm),

168 while the Δ*crtCRT* strain had a reduced VAC size (0.46 ± 0.02 μm) compared to that of WT parasites **(Fig**
169 **1F**). If we assume the shape of the VAC is a sphere, the VAC in Δ*crt* parasites is approximately 15-fold
170 larger in volume than that of WT parasites. In contrast to pulse invasion, the swollen concave structure
171 was not observed in Δ*crt* parasites after replication (**Fig 1G**). However, the TgCPL staining showed
172 differences between WT and Δ*crt* parasites (**Fig 1G**). As a dynamic organelle, the VAC fragments during
173 replication and TgCPL exhibits fragmented puncta staining by immunofluorescence microscopy [4].
174 However, TgCPL did not efficiently fragment and formed a major punctum in replicated Δ*crt* parasites.
175 Therefore, the loss of TgCRT altered the morphology and the dynamic property of the VAC in *Toxoplasma*
176 parasites.

177 The VAC is a lysosome-like organelle, participating in the parasite's endolysosomal system. It provides
178 a place for the maturation of TgCPL and delivers activated TgCPL to its adjacent endosome-like
179 compartment (ELC) to help process certain micronemal proteins required for parasite invasion [4]. It also
180 serves as a digestive vacuole to digest endocytosed proteins [4,11] [20]. Therefore, the dramatic swelling
181 of the VAC could affect the integrity of the parasite's endolysosomal system. We stained WT, Δ*crt*, and
182 Δ*crtCRT* parasites with antibodies recognizing markers of the VAC (anti-TgCPL) and the ELC (anti-
183 proTgM2AP or TgVP1) [4]. During pulse invasion, the VAC and ELC displayed distinct subcellular staining
184 in WT and Δ*crtCRT* strains, whereas both markers partially co-localized in Δ*crt* parasites **(Fig 1G).** Similarly,
185 the major punctum of TgCPL in replicated Δ*crt* parasites also showed partial co-localization with both
186 proTgM2AP and TgVP1 (**Fig 1G**). These findings suggest that the TgCRT plays an essential role in
187 regulating the morphology of the VAC in *T. gondii*, further affecting the integrity of the parasite's
188 endolysosomal system.

189 **3. TgCRT-null mutant displays reduced invasion and acute virulence.**

190 *Toxoplasma* parasites utilize their endolysosomal system to perform exocytosis and endocytosis to
191 release invasion effectors, such as microneme and rhoptry proteins, for their host entry and ingest host
192 proteins for their intracellular growth, respectively [11,21-23]. We characterized invasion, replication, and
193 egress steps individually to understand how the arrested co-localization of the VAC and ELC affects the
194 lytic cycle of *Toxoplasma* parasites. First, we measured the invasion efficiency of parasites at 30 - 120 min

195 post-infection. At 30 min post-infection, the Δ*crt* mutant showed ~50% reduction in invasion compared to
196 WT and Δ*crtCRT* **(Fig 2A)**. The differences in invasion efficiency between WT and Δ*crt* were reduced to
197 ~20% at 60 min post-infection, and were not seen at 120 min post-infection **(Fig 2A)**, suggesting that Δ*crt*
198 parasites have slower kinetics in invasion than the WT strain, but are still able to invade. Second, we
199 conducted immunofluorescence microscopy to quantify parasite replication by counting the numbers of
200 different-sized parasitophorous vacuoles (PVs). The infected cells were stained with DAPI and anti-
201 TgGRA7 antibodies to help recognize the nuclei of individual parasites and the membranes of
202 parasitophorous vacuoles, respectively. The average number of parasites per PV was also calculated in
203 each strain to compare replication rates. There were no significant differences in parasite replication
204 between WT and Δ*crt* parasites at 28 and 40 hrs post-infection **(Fig 2B)**. We also introduced NanoLuc®
205 luciferase into WT, Δ*crt*, and Δ*crtCRT* parasites, and measured the fold-change of their luciferase activities
206 at 72 hrs post-infection to calculate their growth rates. Similarly, we did not observe growth differences
207 between WT and Δ*crt* at 24, 48, and 72 hrs post-infection **(Fig 2B)**. Third, the egress efficiency of each
208 strain was determined by a lactate dehydrogenase release-based assay. The parasites were incubated
209 with 0.5 mM Zaprinast for 5 min to induce egress. The egressed parasites disrupted host cell membranes
210 to release lactate dehydrogenase that was subsequently quantified to reflect the number of egressed PVs.
211 We did not observe egress defects in the TgCRT-deficient parasites **(Fig 2C)**. Last, we determined the
212 acute virulence of Δ*crt* parasites in a murine model. The outbred CD-1 mice were infected with a
213 subcutaneous or intravenous inoculum of 100 WT, Δ*crt*, or Δ*crtCRT* parasites. Thirty percent of mice
214 infected with the Δ*crt* mutant survived when mice were infected by subcutaneous injection, while the WT
215 and Δ*crtCRT* infections led to the mortality of mice in 10-12 days post-infection **(Fig 2D)**. Similarly, the
216 mice receiving WT parasites by intravenous inoculation showed mortality starting at 13 days post-infection
217 and all were dead in 20 days. The Δ*crt* and Δ*crtCRT* parasites caused death in 40% and 80% of infected
218 mice, respectively **(Fig 2D)**. The ability of Δ*crt* parasites to survive in the host was statistically higher than
219 that of WT parasites, regardless of the mode of inoculation. The statistical analysis showed that the mice
220 infected with WT and Δ*crt* parasites showed significantly different survival curves. Seroconversion of the
221 surviving mice was confirmed by ELISA. We also challenged the surviving mice with 1000 WT parasites

222 by subcutaneous injection, and did not observe lethality after 30 days post-challenge. These findings
223 indicate that the pre-inoculation of Δ*crt* parasites conferred immunological protection to the subsequent
224 acute toxoplasmosis. Collectively, our findings revealed that *Toxoplasma* parasites require the TgCRT
225 protein for optimal invasion and acute virulence but not for replication and egress.

226 **4. Microneme secretion is impaired in the Δ*crt* mutant.**

227 During infection, *Toxoplasma* parasites sequentially secrete proteins to facilitate host invasion. The
228 micronemal proteins are the first secreted among these invasion effectors. Micronemal proteins traffic
229 through the parasite's endolysosomal system and undergo intracellular maturation, intramembrane
230 cleavage, and cell surface trimming before reaching their final forms, which facilitate invasion [3-9]. To test
231 which step(s) was/were affected in the Δ*crt* parasites, we probed cell lysates and excretory secretory
232 antigen (ESAs) fractions of each strain with anti-TgMIC2, TgM2AP, and TgMIC5 (three representative
233 micronemal proteins) by immunoblotting to measure their steady abundances and secretion patterns. The
234 migration patterns of these three micronemal proteins in cell lysates were very similar among the strains.
235 The abundances of the individual micronemal proteins in cell lysates were normalized against the protein
236 level of *Toxoplasma* actin protein by densitometry and plotted for quantification. The expression levels of
237 these micronemal proteins were comparable in the cell lysates of individual strains **(Fig 3A)**. To evaluate
238 the patterns and abundances of the secreted forms, we probed constitutive and induced ESAs with anti-
239 TgMIC2, TgM2AP, and TgMIC5 antibodies. The constitutive and induced ESAs were generated by
240 incubating purified parasites in D3 medium (DMEM medium supplemented with 3% (v/v) cosmic calf serum)
241 for 30 min at 37ºC or D3 medium supplemented with 1% (v/v) ethanol for 2 min at 37ºC, respectively. In
242 the ESAs secreted by WT parasites, TgMIC2 exhibited two bands migrating at 100 kDa and 95 kDa, while
243 TgM2AP showed 4 proteolytically processed polypeptides in addition to the pro- and mature forms.
244 However, TgMIC2 only existed as a 100 kDa band in Δ*crt* parasites. Furthermore, mature TgM2AP was
245 not processed in the constitutive ESAs of the Δ*crt* strain and showed significantly reduced processing in
246 the induced ESAs of Δ*crt* parasites **(Fig 3B)**. The secreted TgMIC5 protein displayed similar migration
247 patterns among all three strains **(Fig 3B)**. The secretion of these micronemal proteins was also quantified
248 by normalizing the relative abundances of the proteins against the amount of secreted TgGRA7, a dense

249 granule protein. The secretion of TgMIC2, TgM2AP, and TgMIC5 were reduced by ~80%, 35%, and 40%,
250 respectively, in the induced ESAs of Δ*crt* parasites, compared to the WT strain. The differences in the
251 amount of microneme secretion were less significant in the constitutive ESAs. Only TgMIC2 secretion was
252 decreased by ~55% in Δ*crt* parasites compared to the WT strain, while TgM2AP and TgMIC5 did not show
253 differences **(Fig 3B)**. To examine whether the abnormal secretion of micronemal proteins alters their
254 intracellular trafficking patterns, following pulse invasion and replication, we stained parasites with TgMIC2
255 and TgM2AP antibodies. Both microneme proteins trafficked to the apical end of the parasites and showed
256 normal staining patterns (**Fig 3C**).

257 Before secretion, some membrane-anchored micronemal proteins are released via proteolytic
258 cleavage by intramembrane rhomboid proteases, such as TgROM4. The deletion of TgROM4 leads to the
259 retention of some micronemal proteins on the parasite's plasma membrane, such as TgMIC2 and TgAMA1
260 (*Toxoplasma* apical membrane antigen 1) [6-9]. To test whether the aberrant endolysosomal system alters
261 the retention of micronemal proteins on the surface of parasites, we stained purified, non-permeabilized,
262 extracellular parasites with anti-TgMIC2 antibody. Immunofluorescence microscopy did not reveal excess
263 TgMIC2 on the plasma membrane of Δ*crt* parasites **(Fig S1)**, suggesting that the reduced secretion of
264 micronemal proteins is not due to inefficient intramembrane cleavage of micronemal proteins on the
265 parasite's plasma membrane.

266 The endosome-like compartment is involved not only in the trafficking of micronemal proteins, but also
267 rhoptry contents [24]. We stained newly invaded and replicated parasites with anti-TgROP7 antibodies to
268 examine the trafficking of rhoptry proteins and the morphology of the rhoptry. The TgROP7 staining
269 revealed typical rhoptry patterns located at the apical end of the parasites (**Fig 3D**), excluding the possibility
270 of aberrant trafficking of rhoptry contents and possible defects in the biogenesis of the rhoptry. Taken
271 together, our data suggest that the invasion defects in Δ*crt* parasites are caused by the inefficient secretion
272 and defective trimming of micronemal proteins, while the abnormal morphology of the VAC does not affect
273 the morphology of the rhoptry and the intracellular maturation, trafficking, and intramembrane cleavage of
274 micronemal proteins.

275 **5. Transcript and protein levels of TgSUB1 are decreased in the TgCRT-deficient parasites.**

276 The inefficient proteolytic processing of TgMIC2 and TgM2AP in the ESAs led us to investigate the
277 abundance of *Toxoplasma* subtilisin 1 (TgSUB1) in the Δ*crt* parasites. A previous publication reported that
278 parasites lacking TgSUB1 showed defective trimming patterns of secreted micronemal proteins, such as
279 TgMIC2 and TgM2AP [3], which are very similar to the secretion patterns seen in the Δ*crt* mutant. Therefore,
280 we quantified the abundance of secreted TgSUB1 in both constitutive and induced ESAs by probing them
281 with anti-PfSUB1 antibody, which was generated against *Plasmodium* SUB1 proteins but cross-reacts with
282 TgSUB1 [25]. Immunoblotting analysis revealed that there was no detectable TgSUB1 in the ESAs of Δ*crt*
283 parasites **(Fig 4A).** Non-permeabilized, extracellular parasites were also stained with anti-PfSUB1 to
284 evaluate the amount of surface-anchored TgSUB1. Similarly, there was no detectable TgSUB1 staining
285 on the plasma membrane of Δ*crt* parasites (**Fig 4B**). These data suggest that TgSUB1 is not efficiently
286 delivered to the surface of parasites in the Δ*crt* mutant.

287 TgSUB1 is a micronemal protein. It passes through the parasite's endolysosomal system and becomes
288 activated during trafficking [3,12]. The aberrant endolysosomal system in Δ*crt* parasites could potentially
289 alter the intracellular trafficking of TgSUB1 to prevent its delivery to the microneme. In addition, the
290 aberrant endolysosomal system could alter the maturation process of TgSUB1 and reduce its expression.
291 To test both possibilities, first, following pulse invasion or replication, we stained parasites with anti-PfSUB1
292 antibodies to examine the intracellular trafficking pattern of TgSUB1. TgMIC5 was also stained as a
293 reference for typical microneme staining. Interestingly, we observed much less TgSUB1 staining in Δ*crt*
294 parasites compared to the WT strain (**Fig 4C**). Next, we quantified the steady protein abundance of
295 TgSUB1 in the cell lysates of parasites by immunoblotting, and found that the total abundance of TgSUB1
296 was decreased by approximately 90% in Δ*crt* parasites compared to WT parasites **(Fig 4D)**. To further
297 understand how TgSUB1 expression was suppressed in the Δ*crt* mutant, we performed qPCR to measure
298 the messenger RNA levels of *TgSUB1* in WT, Δ*crt*, and Δ*crtCRT* parasites. Not only was there a reduction
299 of protein expression in Δ*crt* parasites, but the transcripts of *TgSUB1* were also reduced ~10-fold in
300 *Toxoplasma* parasites lacking *TgCRT* **(Fig 4E)**. Collectively, our findings suggest that the arrested co-
301 localization of the VAC and ELC dramatically decreases the abundance of TgSUB1 protein, which further

302 alters the proteolytic processing of micronemal proteins on the surface of parasites during secretion to
303 ultimately reduce invasion efficiency.

304 **6. The morphological alteration of the VAC led to reduced transcript and protein levels of several**
305 **endolysosomal proteases.**

306 The swollen VAC, and its aberrant co-localization with the ELC in Δ*crt* parasites, could result in the
307 global alteration of gene transcription in order to help the parasites adapt to the sub-optimal
308 microenvironment within their endolysosomal system. We conducted transcriptome sequencing to detect
309 global alteration of gene transcription in WT and Δ*crt* parasites. The differential gene expression analysis
310 identified 102 genes whose transcript levels changed greater than 1.5-fold in the Δ*crt* strain. Forty-six and
311 fifty-six genes had increased and reduced transcripts, respectively (**Fig 5A and Table S1**).

312 Four proteases were among the list of genes showing reduced transcripts in the Δ*crt* mutant, including
313 one putative aminopeptidase N protein (TgAMN, TGGT1_221310), one putative Pro-Xaa serine
314 carboxypeptidase (TgSCP, TGGT1_254010), aspartyl protease 1 (TgASP1, TGGT1_201840), and an ICE
315 family protease-like protein (TgICEL, TGGT1_243298). We validated the transcript levels of these
316 proteases in WT, Δ*crt*, and Δ*crtCRT* strains by quantitative PCR (qPCR), and also quantified the transcript
317 levels of two known VAC luminal proteases, TgCPL and TgCPB. The qPCR analysis showed that the
318 transcript levels of TgAMN, TgSCP, TgASP1, and TgCPB were decreased by 50%, 20%, 47%, and 14%,
319 respectively, in Δ*crt* parasites **(Fig 5B)**. The protein levels of TgCPL and TgCPB were quantified and
320 compared in WT, Δ*crt*, and Δ*crtCRT* parasites by immunoblotting analysis. Although the transcript level of
321 TgCPL did not show any difference between the WT and Δ*crt* strains, the protein abundance of TgCPL
322 decreased by ~25% in the Δ*crt* mutant **(Fig 5C)**. The expression level of TgCPB protease was reduced
323 significantly in Δ*crt* parasites. Both the pro- and mature forms of TgCPB in the Δ*crt* mutant showed reduced
324 abundance compared to WT parasites. The level of mature TgCPB was quantified by densitometry and
325 was found to decrease by ~60% in the TgCRT-null mutant **(Fig 5C)**.

326 To determine the subcellular locations of these down-regulated putative proteases, we endogenously
327 tagged TgAMN and TgSCP with 3xHA and 3xmyc epitope tags at their C-termini, respectively, in WT
328 parasites **(Fig S2)**. After drug-selection, we probed the cell lysates of the tagged strains with anti-HA and

329 anti-myc antibodies, respectively, to confirm their expression. Immunoblotting analysis revealed that the
330 observed molecular weights of both proteins were similar to the predicted sizes based on their primary
331 sequences (**Fig 5D**). Next, the tagged strains were stained with antibodies recognizing their respective
332 epitope tags along with anti-TgCPL and anti-VP1 antibodies to determine their subcellular locations.
333 Immunofluorescence microscopy revealed the subcellular locations of both TgSCP and TgAMN to be in
334 the VAC/ELC (**Fig 5D**). The subcellular location of TgASP1 has been determined in a separate study. By
335 probing WT parasites with polyclonal anti-TgASP1 (recently made in our lab) and anti-TgCPL antibodies,
336 we identified TgASP1 as a new VAC-localizing protease (data not shown since this work is being prepared
337 for another publication). Collectively, our data suggest that the swollen VAC in Δ*crt* parasites causes
338 reduced expression of several endolysosomal proteases at both the transcription and translation levels.
339 Reduced proteolytic activities within the VAC could decrease the production of degraded protein products,
340 thereby limiting the swelling of the VAC.

341 **7. Suppression of proteolysis within the swollen VAC in Δ*crt* parasites partially restores the size of**
342 **the VAC and the separation of organelles within the parasite's endolysosomal system, thereby**
343 **moderately restoring invasion.**

344 Since the parasites lacking TgCRT reduced proteolytic activities within the VAC in order to decrease
345 the production of small solutes, it is expected that the inhibition of proteolysis in the swollen VAC would
346 reduce its size. We tested this hypothesis by chemically and genetically suppressing the proteolysis of the
347 VAC. First, we treated WT, Δ*crt*, and Δ*crtCRT* parasites with 1 μM LHVS, an irreversible inhibitor of the
348 TgCPL protease [19], or with the vehicle control DMSO. TgCPL is a major endopeptidase and is involved
349 in the maturation of micronemal proteins and digestion of host proteins [4,11]. Infected host cells were
350 incubated with LHVS for 48 hrs to allow full inhibition of the TgCPL protease in the parasites. Treated
351 parasites were liberated from host cells and used to infect new host cells for 30 minutes, followed by TgCPL
352 staining to quantify the size of the VAC. As expected, the LHVS-treated Δ*crt* parasites displayed smaller
353 VACs than DMSO-treated Δ*crt* parasites **(Fig 6A)**. The cathepsin B-like protease (TgCPB) is another
354 known VAC-localizing protease, displaying both endo- and exo-peptidase activities [14,19]. Due to its
355 carboxypeptidase activity, it is expected that TgCPB contributes to the generation of small solutes to a

356 greater extent than TgCPL. We genetically deleted *TgCPB* in Δ*crt* parasites using a CRISPR-Cas9 editing
357 tool to generate a Δ*crt*Δ*cpb* double knockout **(Fig 6B)**. The replacement of *TgCPB* with a pyrimethamine
358 resistance cassette was confirmed by PCR and immunoblotting **(Fig 6B)**. The resulting Δ*crt*Δ*cpb* mutant
359 showed a smaller concave subcellular structure compared to the Δ*crt* mutant **(Fig S3)**. The size of the VAC
360 in WT, Δ*crt*, and Δ*crt*Δ*cpb* was quantified based on the TgCPL staining as described above. The size of
361 the VACs in Δ*crt*Δ*cpb* parasites (0.85 ± 0.15 μm) were reduced by ~30% compared to that of Δ*crt* parasites
362 (1.15 ± 0.10 μm) **(Fig 6C)**. The moderate decrease in the size of the VAC in the Δ*crt*Δ*cpb* strain also
363 reduced the number of parasites showing partial overlapping between the VAC and ELC. Approximately
364 44% of Δ*crt*Δ*cpb* parasites showed partial co-localization between TgCPL and proTgM2AP staining
365 compared to 62% in the Δ*crt* strain (**Fig 6D**), but this was still significantly higher than 19% and 25% in WT
366 and Δ*crtCRT* strains, respectively. Moreover, we detected that TgSUB1 showed comparable expression
367 in both the WT and Δ*crt*Δ*cpb* strains (**Fig 6E**). Similarly, TgSUB1 was observed in both constitutive and
368 induced ESA fractions in the Δ*crt*Δ*cpb* parasites (**Fig 6F**). TgM2AP and TgMIC2 were cleaved by TgSUB1
369 in Δ*crt*Δ*cpb*, and their secretion patterns were similar to those seen in the WT strain (**Fig 6F**). These
370 restored phenotypes in the Δ*crt*Δ*cpb* mutant improved the invasion efficiency by ~60% compared to the
371 Δ*crt* strain, although the invasion efficiency was still significantly lower than that of WT parasites **(Fig 6G)**.
372 This set of data exhibits a closely linked association among the size of the VAC, altered morphology of the
373 parasite's endolysosomal system, protein abundance of TgSUB1, and parasite invasion. In summary, our
374 findings strongly suggest a role of TgCRT in the transport of small solutes across the VAC membrane to
375 regulate the osmotic pressure within this organelle and govern the proper segregation of other organelles
376 within the endolysosomal system, which facilitates microneme secretion and parasite invasion. It also
377 indicates that the invasion deficiency exhibited in the Δ*crt* mutant is likely caused by multiple determinants,
378 since the recovery of TgSUB1 expression and micronemal trimming in Δ*crt*Δ*cpb* did not fully reverse the
379 invasion defects.

380 **Discussion**

381 As a eukaryotic, single-celled pathogen, *Toxoplasma* parasites utilize their endolysosomal system to
382 secrete invasion effectors to help disseminate infection. These invasion effectors undergo a series of

383 proteolytic cleavage and trimming to reach their final forms. Therefore, maintenance of the integrity of the
384 endolysosomal system is critical for controlling the secretion of invasion effectors in *Toxoplasma*. The
385 Vacuolar Compartment (VAC) is a lysosome-equivalent structure in the parasites, which harbors an acidic
386 environment and exhibits proteolytic activity. The deletion of a cathepsin L-like protease (TgCPL), a major
387 VAC luminal endopeptidase, leads to invasion, replication, and virulence defects [4,11]. The compromised
388 proteolytic activities within the VAC also result in the inefficient degradation of endocytosed host proteins,
389 suggesting its involvement in endocytic activities within parasites [11]. Sally *et al.* previously reported that
390 a *Toxoplasma* ortholog of the chloroquine resistance transporter (TgCRT) resides in the VAC [15]. The
391 knockdown of TgCRT leads to swelling of the VAC [15]. It is still unknown how the swelling of the VAC
392 affects the parasite's endolysosomal system. The incomplete depletion of the TgCRT protein in the
393 knockdown system limits the ability to fully understand its function in the VAC and its role in parasite
394 infection.

395 In this study, we genetically ablated *TgCRT* in *Toxoplasma*, and the resulting Δ*crt* had a dramatic
396 increase in the size of its VAC, which also aberrantly co-localizes with its adjacent endolysosome-like
397 compartment **(Fig 7)**. A previous study reported that the parasites deliver a minute amount of TgCPL from
398 the VAC to the ELC which contributes to the maturation of some micronemal proteins [4]. The aberrant co-
399 localization of the VAC and ELC could potentially bring excess TgCPL into the ELC, which might interfere
400 with the cleavage of micronemal proteins. Our findings did not reveal abnormal intracellular cleavage or
401 trafficking of micronemal proteins in Δ*crt* parasites, indicating that the ELC may not be a major site for the
402 removal of the propeptide of micronemal proteins. Dogga *et al.* recently documented that aspartic acid
403 protease 3 (TgASP3) localizes in a post-Golgi compartment and serves as a major maturase for invasion
404 effectors [5], suggesting that the cleavage of micronemal proteins by TgCPL in the ELC plays only a minor
405 role in their maturation. We also measured the retention and secretion of micronemal proteins on the
406 parasite's surface and in the medium, respectively, which is executed by TgROM4 and TgSUB1,
407 respectively. We found that the micronemal proteins were not properly trimmed on the surface of the Δ*crt*
408 parasites during their secretion. The patterns of the secreted micronemal proteins that were observed in
409 the Δ*crt* mutant were similar to those seen in Δ*sub1* parasites, which led us to examine the expression of

410 TgSUB1 in Δ*crt* parasites and ESAs. As expected, the protein level of TgSUB1 was decreased on the
411 surface of Δ*crt* parasites and in the medium during secretion. Interestingly, the steady state protein
412 abundance of TgSUB1 was also significantly decreased in the Δ*crt* mutant. Surprisingly, we found that the
413 reduction of TgSUB1 was due to a decrease in the transcription levels of TgSUB1 in the Δ*crt* strain,
414 suggesting that the parasites may utilize a feedback mechanism in order to regulate TgSUB1 expression
415 at the transcriptional stage.

416 TgSUB1 is a micronemal protein which is anchored on the surface of *Toxoplasma* parasites via a GPI
417 anchor. It remains unclear how TgSUB1 becomes activated within *Toxoplasma* parasites. Previous pulse-
418 chase experiments have revealed that TgSUB1 undergoes maturation in a post-ER compartment, and
419 passes through the endolysosomal system before its arrival at the microneme and subsequent secretion
420 [12]. The propeptide region of TgSUB1 carries targeting information which helps to guide the protein to the
421 microneme [26]. The propeptide may also function by binding to active sites of mature TgSUB1 to inhibit
422 its proteolytic activity during trafficking. Co-localization of the VAC and ELC could bring propeptide-bound
423 TgSUB1 to a protease-abundant environment, where non-specific digestion of the propeptide could then
424 lead to increased digestive activities in the VAC and ultimately result in an increase in the osmotic pressure
425 within the hybrid VAC/ELC organelle **(Fig 7)**. During this scenario, the parasites may utilize a feedback
426 mechanism to repress the expression of TgSUB1 in order to alleviate the osmotic pressure and avoid
427 further swelling. Moreover, we also discovered that the Δ*crt* parasites had reduced protein and/or transcript
428 levels of several endolysosomal proteases, including two known VAC proteases, TgCPL and TgCPB.
429 Therefore, the parasites down-regulate a number of endolysosomal proteases to suppress proteolytic
430 activities in the swollen VAC in order to reduce osmotic pressure within the lumen, thereby controlling VAC
431 size and morphology. Among these proteases, TgSUB1 has been shown to be involved in parasite
432 invasion and virulence defects but not replication and egress [3]. Additionally, TgCPL plays a role in
433 parasite invasion by maturating several micronemal proteins [4]. Therefore, the invasion defects exhibited
434 in the Δ*crt* mutant could be due to a multitude of factors.

435 The alteration of transcript levels of endolysosomal proteases in Δ*crt* parasites suggests that the
436 parasites may repress transcription factors or enhance transcription repressors to respond to the increase

437 of the VAC size. RNA-Seq analysis did not reveal any members of an AP2-family of transcription factors
438 that had a change in their transcript levels greater than 1.5-fold. Given that the abundance of transcription
439 factors is generally low in cells, the RNA-seq analysis may not be sensitive enough to detect differences
440 in the transcriptional changes between the WT and Δ*crt* strains. In mammalian cells, the transcription factor
441 EB (TFEB) is a master regulator that drives gene expression for autophagy and lysosome biogenesis [27].
442 The ortholog search against the annotated coding sequences of *Toxoplasma* did not result in the
443 corresponding counterparts, suggesting that the parasites could adopt an alternative strategy to regulate
444 lysosomal gene expression. Interestingly, our differential gene expression analysis identified that the
445 transcript levels of two zinc finger (CCCH) type motif-containing proteins, TGGT1_246200 and
446 TGGT1_226310, were increased and decreased by 2-fold and 3-fold, respectively, in the Δ*crt* mutant. The
447 CCCH type zinc finger motif-containing protein is known to regulate the stability of mRNA [28]. For example,
448 tristetraprolin inhibits the production of tumor necrosis factor-α in macrophages by destabilizing its mRNA
449 via an interaction with its AU-rich elements at the 3'-untranslated region [29]. Further investigation to
450 identify transcription factor(s) and regulator(s) that govern the expression of lysosomal genes will help
451 elucidate how *Toxoplasma* parasites regulate the biogenesis of the VAC.

452 In this study, we determined that the TgCRT-deficient parasites have reduced expression of several
453 endolysosomal proteases. We also found that the suppression of proteolytic activities within the swollen
454 VAC decreases its size. These findings support the idea that CRT functions as an amino acid/peptide
455 transporter to regulate the osmotic pressure inside the digestive vacuole. When TgCRT is absent on the
456 membrane of the VAC, decomposed protein products accumulate within the VAC and increase the osmotic
457 pressure, thereby leading to the swollen phenotype. Chemical inhibition of proteolysis via the small inhibitor
458 LHVS dramatically reduces the size of the VAC. LHVS principally targets TgCPL in the parasites, but also
459 binds to TgCPB protease [14]. Additionally, the maturation of TgCPB is dependent upon the presence of
460 TgCPL [14]. Therefore, the treatment of LHVS blocks both of these VAC proteases. Since the TgCPB
461 protease exhibits endo- and exo-peptidase activities and the deletion of TgCPB had no effect on the
462 abundance of TgCPL [14], we genetically ablated *TgCPB* to understand its role in regulating the
463 morphology of the VAC. The deletion of TgCPB partially restored the size of the VAC, secretion patterns

464 of micronemal proteins, and invasion defects. These results reveal for the first time that TgCPB plays an
465 active role in contributing to proteolysis within the VAC in *Toxoplasma* parasites.

466 Our RNA-Seq analysis also identified several other genes with altered transcription levels, suggesting
467 that the parasites may utilize other strategies to control the size of the VAC. For example, the transcript
468 levels of a water channel protein, aquaporin (TGGT1_215450), was reduced in Δ*crt* parasites. A previous
469 study has reported that this aquaporin protein is localized in the VAC/PLV [30]. Therefore, the Δ*crt*
470 parasites may express less aquaporin to reduce water intake into the VAC/PLV as a tactic to limit the
471 swelling of the organelle. We also found that two putative protein phosphatase 2C orthologs
472 (TGGT1_276920 and TGGT1_201520) became down-regulated in the Δ*crt* mutant. Both of these proteins
473 carry signal peptides, indicating that they traffic through the parasite's endosomal system. Based on a
474 sequence-based ortholog search, TGGT1_276920 and TGGT1_201520 are homologous to PTC3 and
475 PTC1 in *Saccharomyces cerevisiae,* respectively. Interestingly, both PTC1 and PTC3 proteins are involved
476 in the regulation of osmosensing in yeast. A mitogen-activated protein kinase pathway is activated when
477 yeast cells experience hyperosmotic conditions. PTC1 and PTC3 were shown to negatively regulate this
478 pathway [31,32]. Furthermore, PTC1 was found to control the function and morphology of the vacuole in
479 yeast cells, which further alters its biogenesis [33]. The dramatic change in the volume of the VAC could
480 induce osmotic stress in the Δ*crt* parasites. The parasites may utilize a similar mechanism to suppress
481 both of these protein phosphatases, thereby enhancing the activity of a similar signaling pathway to help
482 them adapt to such stress.

483 The phenotype of the swollen VAC in the Δ*crt* strain mirrors the enlarged digestive vacuole in
484 chloroquine (CQ) resistant malaria strains [34]. Thus far, the CRT gene could not be deleted in malaria
485 parasites. Peptidomics analysis showed that hemoglobin cannot be efficiently degraded within the
486 digestive vacuole in CQ resistant malaria parasites [35], suggesting that the mutations in malarial CRT
487 may alter the physiological conditions within the swollen digestive vacuole, thereby also compromising its
488 proteolytic activities. An *in vitro* assay utilizing recombinant malarial CRT proteins that were reconstituted
489 in proteoliposomes revealed that PfCRT acts as a proton gradient dependent, poly-specific nutrient
490 exporter for small solutes, such as amino acids, oligopeptides, glutathione, and small drugs [17]. This study

491 also demonstrated that the PfCRTs derived from the CQ resistant malaria strains displayed less efficient
492 transport of small solutes than their counterpart in the CQ sensitive strain [17]. The alteration of proteolytic
493 activities in the enlarged VAC in the Δ*crt* mutant may reflect a similar scenario that occurred in the digestive
494 vacuole of the CQ resistant malaria parasites. Given the similarity in the components and functionality of
495 digestive vacuoles between *Toxoplasma* and *Plasmodium* parasites, the *Toxoplasma TgCRT*-deficient
496 mutant could be used to study the native role of CRT orthologs in other apicomplexam parasites.
497 Collectively, our findings revealed that the *Toxoplasma* chloroquine resistance transporter plays an
498 important role in regulating the size and morphology of the digestive vacuole in the parasites. This
499 regulation helps to maintain the integrity of the parasite's endolysosomal system, which provides routes
500 for the trafficking of invasion effectors. The co-localization between the digestive vacuole and endosome-
501 like compartment also led to a reduction of the transcript and protein levels of several endolysosomal
502 proteases. We also showed that blocking proteolysis within the swollen digestive vacuole reduced the size
503 and partially restored the morphology of the organelle. These findings suggest that TgCRT mediates the
504 transport of small solutes in order to regulate the size and morphology of the digestive vacuole. Our study
505 provides clear evidence that the integrity of the endolysosomal system in parasites is critical for the
506 virulence of parasites. Therefore, pharmaceutical modulation of the digestive vacuole could potentially
507 serve as a novel strategy to manage toxoplasmosis.
508

509 **Materials and Methods**

510 **Ethical statement**

511 This study was performed in compliance with the Public Health Service Policy on Humane Care and
512 Use of Laboratory Animals and Association for the Assessment and Accreditation of Laboratory Animal
513 Care guidelines. The animal protocol was approved by Clemson University's Institutional Animal Care and
514 Use Committee (Animal Welfare Assurance A3737-01, protocol number AUP2016-012). All efforts were
515 made to minimize discomfort. This method of euthanasia is consistent with the recommendations of the
516 Panel on Euthanasia of the American Veterinary Medical Association.

517 **Chemicals and reagents**

518 Morpholine urea-leucyl-homophenyl-vinyl sulfone phenyl (LHVS) was kindly provided by the Bogyo
519 lab at Stanford University. Other chemicals used in this work were analytical grade and were purchased
520 from VWR unless otherwise indicated.

521 **Parasite culture**

522 *Toxoplasma gondii* parasites were cultured in human foreskin fibroblast (HFF) cells (ATCC, SCRC-
523 1041) in Dulbecco's Modified Eagle Medium (DMEM) media supplemented with 10% cosmic calf serum at
524 37 °C with 5% CO_2. The parasites were harvested by membrane filtration as described previously [14].

525 **Generation of transgenic parasites**

526 To generate the TgCRT-deficient strain, ~1.5 kilobases (kb) of 5'- and 3'-UTR (untranslated region) of
527 the *TgCRT* gene, respectively, were PCR-amplified and flanked at both ends of the bleomycin resistance
528 cassette (BLE) to assemble a *TgCRT* deletion construct. The resulting plasmids were introduced into WT
529 parasites by electroporation. The transfected parasites were selected with 50 µg/ml bleomycin twice, while
530 in their extracellular stage as described previously [14]. The clones of the TgCRT-deficient parasites were
531 generated by limiting dilution in a 96-well plate. The correct replacement of *TgCRT* with the *BLE* cassette
532 was confirmed by PCR and quantitative PCR.

533 To complement the TgCRT in Δ*crt* parasites, we modified the plasmid, named pTub-TgCRT-mCherry-
534 3xmyc (a gift from the van Dooren lab), which expresses a C-terminally mCherry-3xmyc epitope-tagged
535 TgCRT under the *Toxoplasma* tubulin promoter. The plasmid was cut with HpaI and MfeI restriction

536 enzymes to remove the tubulin promoter and a partial sequence of TgCRT. The remaining DNA fragment
537 served as the backbone for the subsequent Gibson assembly to incorporate the PCR amplified ~1 kb
538 region upstream of the *Tgku80* gene, the ~1 kb fragment of the *Tgcrt* 5'-UTR region, and the removed
539 partial *Tgcrt* coding sequence to produce the TgCRT complementation plasmid, pCRT-TgCRT-mCherry-
540 3xmyc. The complemented TgCRT is driven by its cognate promoter to keep its expression level similar to
541 the native TgCRT expression in WT parasites. The 1 kb region located ~6 kb upstream of the *Tgku80* gene
542 was used to facilitate a single integration of the TgCRT complementation plasmid into this specific locus
543 by single crossover homologous recombination. The TgCRT complementation construct was digested with
544 SwaI restriction enzyme, gel-extracted, purified, and transfected into Δ*crt* parasites by the standard
545 electroporation protocol.

546 To introduce NanoLuc® luciferase (nLuc) into parasites, we PCR-amplified and assembled the
547 *Tgtubulin* promoter, the coding sequence of the nLuc luciferase, and an HXG selection marker into a nLuc
548 expression construct by standard molecular cloning. The resulting plasmids were transfected into WT, Δ*crt*,
549 and Δ*crtCRT*. The transfectants were selected with 25 µg/ml mycophenolic acid and 50 µg/ml xanthine.
550 The stable populations were subjected to limiting dilution to generate individual clones of WT::*nLuc*,
551 Δ*crt*::*nLuc*, and Δ*crtCRT*::*nLuc*. The correct clones were confirmed by their luciferase activities.

552 To generate the Δ*crt*Δ*cpb* mutant, the *TgCPB* gene was replaced with a pyrimethamine resistance
553 cassette using the CRISPR-Cas9 genome editing system [36,37]. The pyrimethamine resistance cassette
554 was PCR-amplified and flanked by 50 bp regions upstream and downstream of the start and stop codons
555 of the *TgCPB* gene for homologous recombination. A 20 bp region located at the beginning of the coding
556 region of the *TgCPB* gene was used to design guide RNA and replace the guide RNA targeting TgUPRT
557 gene in the plasmid pSAG1-Cas9::UPRTsgRNA using Q5 site-directed mutagenesis kit (NEB). The Cas9-
558 GFP and guide RNA constructs were co-transfected into Δ*crt* parasites with the corresponding repair PCR
559 product. The guide RNA and Cas9 generated a gap within the *TgCPB* gene in the genome to facilitate
560 double crossover homologous recombination. The correct gene replacement was confirmed by PCR.
561

562 To endogenously epitope-tag TgAMN, we also used CRISPR-Cas9 editing tools to modify the
563 corresponding gene in the genome. Guide RNA recognizing the 20 bp region close to the stop codon of
564 TgAMN was generated using the methods mentioned above.

565 The 50-bp homologous regions upstream and downstream of the stop codon of the *TgAMN* gene was
566 cloned at 5'- and 3'-ends of the DNA sequence containing the 3xHA epitope tag and the pyrimethamine
567 resistance cassette, respectively, by PCR. The plasmid encoding the guide RNA targeting TgAMN and
568 Cas9-GFP and the PCR product were co-trasfected into WT parasites. The stop codon of TgAMN was
569 replaced by the 3xHA epitope tag and pyrimethamine resistance cassette. The stable population was
570 generated after multiple rounds of pyrimethamine selection. The TgAMN-3xHA fusion protein was
571 confirmed by immunoblotting analysis.

572 TgSCP was endogenously tagged with a 3xmyc epitope tag via the single crossover recombination.
573 Approximately a 1 kb upstream region of the stop codon of the *TgSCP* gene was amplified by PCR and
574 fused in frame with a 3xmyc epitope tag at its 5'-end to assemble a TgSCP-3xmyc tagging construct. A
575 pyrimethamine resistance cassette was also encoded in the construct for drug selection. The resulting
576 plasmid was linearized by the restriction endonuclease NarI within the 1 kb region of the *TgSCP* gene prior
577 to transfection into WT parasites. The 3xmyc epitope tag was incorporated at the end of the *TgSCP* gene.
578 The correct tagging was confirmed by immunoblotting analysis.

579 **Transfection of *Toxoplasma* parasites**

580 *T. gondii* parasites were allowed to grow in HFF cells for 48 hrs at 37 °C with 5% CO_2. The freshly
581 egressed parasites were syringed, filter purified, and harvested in Cytomix buffer (25 mM HEPES, pH 7.6,
582 120 mM KCl, 10 mM K_2HPO4/ KH_2PO4, 5 mM $MgCl_2$. 0.15 mM $CaCl_2$, and 2 mM EGTA). Parasites were
583 pelleted at 1,000x *g* for 10 min, washed once in Cytomix buffer, and resuspended in Cytomix buffer at 2.5
584 x 10^7 parasites per ml. The 400 µL parasite suspension was mixed with 20 µg DNA and 2 mM ATP/5 mM
585 reduced glutathione for a total volume of 500 µl. The mixture was electroporated at 2 kV and 50 ohm
586 resistance using the BTX Gemini X2 (Harvard Apparatus). The transfected parasites were inoculated into
587 a T25 flask pre-seeded with a confluent monolayer of HFF cells. The corresponding drug selection was
588 applied at 24 hrs post-transfection.

589 **Immunofluorescence assay**

590 To perform immunofluorescence of intracellular parasites, freshly lysed parasites were used to infect
591 confluent HFF cells pre-seeded in an 8-well chamber slide for 1 hr (pulse invasion) or 18-24 hrs
592 (replication). The extracellular parasites were glued onto chamber slides by using 0.1% (w/v) poly-L-lysine
593 before staining. Immunofluorescence staining was performed as described previously [11,14]. Images
594 were viewed and digitally captured using a Leica® CCD camera equipped with a DMi8 inverted
595 epifluorescence microscope and processed with Leica® LAS X software. Adobe Photoshop software was
596 used to assemble the final images.

597 **Excretory secretory antigens (ESAs) preparation**

598 Freshly egressed parasites were syringed, filter purified, and resuspended at 5 x 10^8 parasites/ml in
599 D3 medium (DMEM medium supplemented with 3% FBS). One hundred microliters of parasite suspension
600 was transferred to a microfuge tube and incubated at 37 °C for 30 min to prepare constitutive ESAs. To
601 make induced ESAs, the parasite resuspension was incubated in D1 medium supplemented with 1%
602 ethanol for 2 min at 37ºC. The ESAs were separated from intact parasites by centrifugation at 1,000 x *g*
603 for 10 min. The ESA fractions were transferred to a new microfuge tube, mixed with SDS-PAGE sample
604 loading buffer, and boiled for 5 min for immunoblotting analysis.

605 **SDS-PAGE electrophoresis and immunoblotting analysis**

606 Parasite lysates and ESA fractions were prepared in 1x SDS-PAGE sample buffer and boiled for 5 min
607 before resolving on SDS-PAGE gels and transferring to PVDF membranes by semi-dry protein transfer
608 methods. Blots were blocked with 5% non-fat milk and incubated with primary antibodies diluted in 1%
609 non-fat milk. Goat anti-mouse or anti-rabbit IgG antibodies conjugated with horseradish peroxidase were
610 used as the secondary antibodies. Immunoblots were developed with SuperSignal™ WestPico
611 chemiluminescent substrate (Thermo). The chemiluminescence signals were captured using the Azure®
612 Imaging System. The densitometry and quantification of the protein bands were quantified by using LI-
613 COR® Image Studio software.

614 **Parasite invasion assay**

615 Red-green invasion assay was used to measure the efficiency of parasite invasion. Freshly purified
616 parasites were syringed, filter purified, and resuspended at 5 x 10^7 parasites/ml in invasion medium (DMEM
617 supplemented with 3% FBS). Two hundred microliters of the parasite resuspension was inoculated into
618 each well of an 8-well chamber slide pre-seeded with HFF cells, and the parasites were allowed to invade
619 host cells for 30, 60, and 120 min before fixation with 4% formaldehyde for 20 min. Before membrane
620 permeabilization, slides were stained with mouse anti-TgSAG1 monoclonal antibody (1:1,000) for 1 hr to
621 label attached parasites. After treatment with 0.1% Triton X-100 for 10 min, the parasites were stained with
622 rabbit polyclonal anti-TgMIC5 antibody (1:1,000) for 1 hr to stain both invaded and attached parasites.
623 Subsequently, slides were stained with goat anti-mouse IgG conjugated with Alexa 594 (red) (Invitrogen,
624 1:1,000) and goat anti-rabbit IgG conjugated with Alexa 488 (green) (Invitrogen, 1:1,000) along with DAPI
625 for nucleus staining. After staining, slides were mounted with anti-fade Mowiol solution and observed by
626 immunofluorescence microscopy. Extracellular parasites only showed red fluorescence, whereas
627 intracellular parasites exhibited both red and green fluorescence. Six fields of view from individual invasion
628 experiments were captured by the Leica® DMi8 inverted epifluorescence microscope and enumerated by
629 ImageJ software. The attachment efficiency of each strain was measured by dividing the total number of
630 parasites labeled in red by the total number of host nuclei, and normalized against that of WT parasites.
631 The invasion efficiency of each strain was quantified using the following equation (the sum of parasites
632 labeled in green − the sum of parasites labeled in red)／the total number of host nuclei, and normalized
633 against that of WT parasites.

634 **Immunofluorescence-based replication assay**

635 Freshly egressed parasites were filter-purified and inoculated into individual wells of an 8-well chamber
636 slide pre-seeded with HFF cells at approximately 1 x 10^5 cells per well. Non-invaded parasites were
637 washed off at 4 hrs post-infection. Invaded parasites were allowed to infect host cells for an additional 24
638 and 36 hrs before fixation. The infected host cells were stained with monoclonal anti-TgGRA7 (1:2,000)
639 antibody and DAPI to help distinguish individual parasitophorous vacuoles (PVs) and the nuclei of
640 parasites, respectively. Slides were subjected to standard immunofluorescence microscopy for imaging.
641 One hundred parasitophorous vacuoles were enumerated for each strain and plotted as the distribution of

642 different sized PVs. In addition, replication was also expressed as the average number of parasites per
643 PV.

644 **Luminescence-based growth assay**

645 Parasites expressing NanoLuc luciferase were inoculated into a white 96-well tissue culture plate with
646 a flat, solid bottom (Greiner Bio-One) pre-seeded with confluent HFF cells at 1.5 x 10^3 cells/well. Each
647 strain was inoculated into 4 individual wells to monitor the fold-change of luciferase activities over a time
648 course, which reflects intracellular growth of the parasites. After 4 hrs post-infection, the individual wells
649 were aspirated to remove non-invaded parasites. The first well was treated with 100 µl of lysis buffer
650 containing NanoLuc luciferase substrate and incubated for 10 min, and a luminescence reading was taken
651 by using the BioTek® multimode H1 hybrid plate reader. The rest of the 3 wells were replenished with fresh
652 D10 medium without phenol red for an additional 24, 48, and 72 hrs. The subsequent luminescence
653 readings were all determined using the methods mentioned above. The luminescence readings at different
654 time intervals were normalized against the reading at 4 hrs post-infection to calculate the fold-change of
655 parasite growth.

656 **Egress assay**

657 Lactate dehydrogenase release assay was used to measure the egress efficiency of parasites. Freshly
658 lysed parasites were filter-purified and resuspended in D10 medium at 5 x 10^5 parasites/ml. One hundred
659 microliters of the parasite resuspension was inoculated into each well of a 96-well plate pre-seeded with
660 HFF cells. The parasites were allowed to replicate for 18-24 hrs, washed, and incubated with 50 µl of
661 Ringer's buffer (10 mM HEPES, pH 7.2, 3 mM HaH_2PO_4, 1 mM $MgCl_2$, 2 mM $CaCl_2$, 3 mM KCl, 115 mM
662 NaCl, 10 mM glucose, and 1% FBS) for 20 min. Subsequently, an equal volume of 1 mM Zaprinast
663 dissolved in Ringer's buffer was added into the wells and incubated for 5 min at 37ºC and 5% CO_2.
664 Uninfected wells were treated with 50 µl of Ringer's buffer containing 1% Triton X-100 or plain Ringer's
665 buffer, serving as positive and negative controls, respectively. The released lactate dehydrogenase was
666 centrifuged at 1,000 *x g* for 5 min twice to pellet insoluble cell debris. Fifty microliters of supernatant was
667 subjected to the standard lactate dehydrogenase release assay as described previously [38]. The egress
668 efficiency of each strain was calculated using the following equation, (LDH activity derived from individual

669 parasites − LDH activity of negative control)／(LDH activity of positive control − LDH activity of negative
670 control), and normalized against that of WT parasites.

671 **Size measurement of the VAC**

672 The size of the VAC was quantified based on the staining of TgCPL, a VAC luminal protease. Freshly
673 purified parasites were inoculated into pre-seeded HFF chamber slides, allowed to invade host cells for 30
674 min prior to fixation, stained with polyclonal rabbit anti-TgCPL antibody (1:100), and subjected to standard
675 immunofluorescence microscopy. The distance of the widest diagonal of the TgCPL staining was
676 determined as the diameter of the VAC and was measured using the Leica® LAS X software.
677 Measurements of 50 individual parasites were performed for each replicate.

678 **Transcriptome sequencing and quantitative PCR (qPCR) assay**

679 Total RNA was extracted from freshly lysed parasites using the Zymo® Direct-zol™ RNA MiniPrep Plus
680 kit, and converted to sequencing read libraries by using the TruSeq Stranded mRNA sequencing kit
681 (Illumina). The prepared libraries were subjected to 2 x 125 bp paired-end Illumina® HiSeq2500 sequencing.
682 Each sample was sequenced to a depth of at least 20 million reads. Differential expression profiling was
683 performed by the Clemson University Genomics Computational Lab.

684 Approximately 500 ng of total RNA was used to measure the steady levels of transcripts for individual
685 genes by using the Luna® Universal One-Step RT-PCR kit (NEB). The qPCR assay was performed using
686 the BioRad CFX96 Touch™ Real-Time PCR detection system. The quantification cycle (Cq) values for
687 individual genes were used for double delta Cq analysis to calculate their relative abundances to that of
688 WT parasites using the Bio-Rad® CFX Maestro™ software. TgActin was used as the housekeeping gene
689 for normalization.

690 **Mouse studies**

691 Six- to eight-week-old, outbred CD-1 mice were infected by subcutaneous or intravenous injection with
692 100 WT or mutant parasites diluted in PBS. The infected mice were monitored for symptoms daily for a
693 total of 30 days. Mice that appeared moribund were humanely euthanized via CO_2 overdose, in compliance
694 with IACUC's approved protocol. The seroconversion of the surviving mice was tested by enzyme-linked
695 immunosorbent assay (ELISA). The surviving mice were allowed to rest for 10 days, prior to subcutaneous

696 injection with a challenge dose of 1000 WT parasites, and were monitored daily for survival for 30 days.

697 **Cloning and Expression of the recombinant pro-form of TgASP1**

698 A ~1.5-kb DNA fragment encoding the recombinant pro-form of TgASP1 (rproTgASP1) was PCR-
699 amplified from a *T. gondii* RH cDNA library using Q5® High-Fidelity DNA polymerase (New England Biolabs)
700 and cloned into a pET22b vector. A 6xHis epitope tag was fused in-frame at the N-terminal end of TgASP1.
701 The resulting pET22b-6xHis-TgASP1 expression construct was transformed into the *E. coli* protein
702 expression strain, ER2566 (NEB). Recombinant TgASP1 was induced with 1 mM isopropyl 1-thio-β-D-
703 galactopyranoside (IPTG) at 37ºC for 4 hrs. The expressed recombinant TgASP1 protein was purified
704 using a standard denature protein purification procedure of recombinant His-tagged proteins as described
705 previously [19]. The purified denatured TgASP1 protein was refolded in phosphate buffered saline (PBS)
706 buffer overnight by dialysis. Mis-aggregated TgASP1 was removed by centrifugation at 20,000 *xg* for 10
707 min. The soluble fraction was concentrated using an Amicon® Ultra 30-kDa cutoff concentrator (Millipore)
708 and stored at -20ºC for future use.

709 **Antibody Preparation**

710 The purified pro-forms of TgASP1 were shipped to Cocalico Biologicals, Inc. to generate polyclonal
711 antibodies. Two New Zealand white rabbits were initially injected with 200 µg of purified recombinant
712 protein in Freund's complete adjuvant and boosted 3 times at Day 14, 21, and 56 with 50 µg of recombinant
713 protein in Freund's incomplete adjuvant. The specificity of the polyclonal antibodies were assessed by
714 comparing their reactivity in WT and Δ*asp1* parasites by immunoblotting and immunofluorescence assay.

715 **Statistics**

716 Statistical analysis was performed using Prism software (GraphPad). The methods used in different
717 assays were indicated in the figure legends.

718

Data Availability Statement: The raw data of transcriptomic sequencing of WT and Δ*crt* strains have been deposited in the NIH Gene Expression Omnibus (GEO) database. The accession number is GSE116539. https://www.ncbi.nlm.nih.gov/geo/query/acc.cgi?acc=GSE116539

Funding: This work was supported by Knights Templar Eye Foundation Pediatric Ophthalmology Career-Starter Research Grant (to Z.D.), a pilot grant of an NIH COBRE grant P20GM109094 (to Z.D.), and the Clemson Startup fund (to Z.D.). The funders had no role in study design, data collection and analysis, decision to publish, or preparation of the manuscript.

Competing Interests: The authors have declared that no competing interests exist.

Acknowledgments

We thank our colleagues Drs. Michael Blackman, Peter Bradley, Vern Carruthers, Silvia Moreno, and David Sibley for kindly providing key reagents for this study. We also want to thank Drs. Rooksana Noorai and Vijay Shankar at Clemson University Genomics Computational Lab for providing technical assistance and expertise in performing transcriptomic sequencing and differential gene expression analysis and depositing the raw data files of transcriptomic sequencing into the NIH GEO database. We acknowledge Dr. Lesly Temesvari for critically reading this manuscript before submission.

Author Contributions

Conceptualization: Zhicheng Dou.

Formal analysis: L. Brock Thornton, Paige Teehan, Katherine Floyd, Christian Cochrane, Amy Bergmann, Zhicheng Dou.

Funding acquisition: Zhicheng Dou.

Investigation: L. Brock Thornton, Paige Teehan, Katherine Floyd, Christian Cochrane, Amy Bergmann, Zhicheng Dou.

Methodology: L. Brock Thornton, Paige Teehan, Zhicheng Dou.

Project administration: Zhicheng Dou.

Resources: Paige Teehan, Amy Bergmann, Zhicheng Dou.

Supervision: Zhicheng Dou.

Writing – original draft: Zhicheng Dou.

Writing – review & editing: L. Brock Thornton, Zhicheng Dou.

Figure legends:

Figure 1. The TgCRT-deficient parasites displayed a swollen digestive vacuole and a disrupted endolysosomal system. A) Schematic illustration of the strategies for the *Tgcrt* deletion and complementation in *Toxoplasma* parasites. The plasmid carrying a bleomycin resistance cassette (*BLE*) flanked by the *TgCRT* targeting sequences was transfected into WT parasites for double crossover replacement of *TgCRT* to produce the Δ*crt* strain. The TgCRT complementation plasmid, containing the coding sequence of TgCRT fused with mCherry and 3xmyc epitope tags at its C-terminus, was introduced into the Δ*crt* strain to produce the Δ*crtCRT* complementation strain. **B)** The primers indicated in panel A were used to verify the correct replacement of *TgCRT* with *BLE* by PCR. **C)** The complemented *TgCRT* gene was transfected into Δ*crt* parasites and was verified by PCR. Since we complemented Δ*crt* with the coding sequence of *TgCRT*, the PCR product was a 0.2 kb fragment in the Δ*crtCRT* strain, whereas the WT strain showed a 1.5 kb product since its *TgCRT* gene contains the introns. **D)** Transcript levels of *TgCRT* in the WT, Δ*crt*, and Δ*crtCRT* strains were evaluated by quantitative PCR. Primers were designed to anneal to the exons of *TgCRT* and are indicated in Panel A. The *Tgactin* gene was included as a control for normalization. The quantification of transcripts was performed in at least three biological replicates and analyzed using unpaired Student's *t*-test. **E)** Extracellular Δ*crt* parasites showed an enlarged concave subcellular structure, indicated by the arrow, under the differential interference contrast (DIC) microscopy. Scale bar = 5 μm. **F)** The swollen subcellular structure indicated by the arrowhead was also observed in Δ*crt* parasites during pulse invasion and co-localized with a major luminal peptidase of the VAC, cathepsin L-like protease (TgCPL). The TgCPL staining was used to assess the morphology of the VAC. The parasites were allowed to invade host cells for 30 min before TgCPL antibody staining. The distance of the widest diagonal of the TgCPL staining was determined to be the diameter of the VAC and was measured using the Leica® LAS X software. The measurements were conducted in three biological replicates. Measurements from 50 individual parasites from one representative assay were shown. The mean VAC size ± SD was calculated for three independent measurements and is listed on the figure. Statistical significance was determined using unpaired Student's *t*-test. Scale bar = 2 μm. **G)** Parasites were co-stained with anti-TgCPL (the marker of the VAC) and anti-proM2AP or anti-TgVP1 (both are markers of

the endosome-like compartment, ELC). During pulse invasion, the VAC and ELC staining were juxtaposed in the WT and Δ*crtCRT* strains, but aberrantly co-localized in the Δ*crt* strain. During replication, the VAC in WT and Δ*crtCRT* parasites became fragmented. However, the abnormal co-localization of the VAC and ELC significantly decreased the extent of VAC fragmentation in the Δ*crt* mutant. A major TgCPL punctum existed in the replicated Δ*crt* parasites, not in WT and Δ*crtCRT* strains, and co-localized with proTgM2AP and TgVP1 (indicated by arrows in the insets). The scale bars in the images of parasites at the stages of pulse invasion and replication are 2 μm and 5 μm, respectively. ****, $p<0.0001$; n.s., not significant.

Figure 2. Parasite invasion and acute virulence were reduced in the Δ*crt* parasites. A) WT, Δ*crt*, and Δ*crtCRT* parasites were allowed to invade host cells for 30, 60, and 120 min prior to fixation and antibody staining. Parasites and host cells within six fields of view were counted for each strain. At least three independent invasion assays were conducted for statistical analysis. The Δ*crt* parasites showed a ~50% reduction in invasion at 30 min post-infection. The extent of the invasion defect in the Δ*crt* mutant was gradually minimized overtime. At 60 min post-infection, there was approximately a 25% reduction in invasion in the Δ*crt* mutant, while there were no significant differences among the three strains at 120 min post-infection. The assay was performed at least in triplicate. Statistical significance was determined using unpaired Student's *t*-test. **B)** We infected confluent HFFs with WT, Δ*crt*, and Δ*crtCRT* parasites for 28 and 40 hrs before fixation and staining. Infected cells were stained with DAPI and anti-TgGRA7 antibodies in order to recognize individual parasites and parasitophorous vacuoles, respectively. One hundred parasitophorous vacuoles (PVs) were enumerated for the number of parasites they contained and the distribution of different sized PVs was plotted. The average number of parasites per PV was also calculated and listed above the plots. In addition, the growth rates of these strains were determined at 24, 48, and 72 hours by using a luminescence-based assay. Parasites were inoculated into a 96-well plate pre-seeded with HFFs prior to lysis and quantification of luminescence activities at pre-determined time intervals. At least three biological replicates were performed for the replication assay. Unpaired Student's *t*-test was performed to calculate the statistical significance of parasite growth between strains. **C)** To measure the egress of the parasites, 5×10^4 parasites were used to infect confluent HFFs in a 96-well plate for 24 hrs.

Replicated parasites were treated with 500 μM Zaprinast for 5 min at 37ºC and 5% CO_2 to induce egress. Disruption of host cell membranes due to parasite egress released lactate dehydrogenase into the medium, which was quantified and plotted. Unpaired Student's *t*-test was used to calculate the statistical significance. There were no differences observed in parasite egress between WT and Δ*crt* parasites. **D)** The acute virulence of TgCRT-deficient parasites was evaluated in a murine model via subcutaneous and intravenous infections. One hundred parasites from each strain were used to infect outbred CD-1 mice (n=10 mice for each strain). The mortality of the mice was monitored for 30 days. Seroconversion of the surviving mice was evaluated by ELISA to confirm successful infection. Additionally, the surviving mice were allowed to rest for 10 days before subsequent challenge with 1,000 WT parasites by subcutaneous inoculation. The Δ*crt* mutant exhibited reduced acute virulence compared to the WT and Δ*crtCRT* strains and conferred immunological protection in the surviving mice. Data were recorded and are presented using the Kaplan-Meier plot. Statistical analysis was performed using the Log-rank (Mantel-Cox) test. For all statistical significance calculations, *, $p<0.05$; **, $p<0.01$; ****, $p<0.0001$; n.s, not significant.

Figure 3. The deletion of *TgCRT* altered microneme secretion, without affecting the microneme steady abundance, intracellular trafficking, and intramembrane cleavage on the parasite surface. A) The steady levels of micronemal proteins were not altered in the Δ*crt* parasites. Freshly lysed parasites were filter-purified, lysed, and subjected to SDS-PAGE electrophoresis and immunoblotting. The blots were probed with anti-TgMIC2, TgM2AP, and TgMIC5 antibodies, along with anti-TgActin as the loading control. Individual micronemal proteins were normalized against the corresponding TgActin to quantify their steady state expression. **B)** Δ*crt* parasites secreted less micronemal proteins than WT and Δ*crtCRT* parasites, and altered the micronemal secretion patterns. Freshly filter-purified parasites were incubated in medium at 37ºC for 30 min to make constitutive ESAs or were treated with 1% (v/v) ethanol in medium to produce induced ESAs. The ESA fractions were separated and probed with anti-TgMIC2, TgM2AP, and TgMIC5 antibodies for quantification of the secreted forms of these micronemal proteins. The ESA fractions were also probed with anti-TgGRA7 antibody, a dense granule protein, as the loading control. Statistical significance was determined using unpaired Student's *t*-test. **C)** Following pulse invasion and replication,

the parasites were stained with anti-TgMIC2 and anti-TgM2AP antibodies to examine their intracellular trafficking. No defects were detected in their intracellular trafficking. **D)** The parasites at the stages of pulse invasion and replication were also stained with anti-TgROP7 to examine the morphology of the rhoptry and intracellular trafficking of TgROP7. Similar morphology and trafficking patterns of the rhoptry were maintained among WT, Δ*crt*, and Δ*crtCRT* strains. The scale bars in the images of parasites during pulse invasion and at extracellular stage are 2 μm, and the scale bar in the images of replicated parasites is 5 μm. *, $p<0.05$; **, $p<0.01$; ***, $p<0.001$; ****, $p<0.0001$; n.s., not significant.

Figure 4. The transcript and protein levels of a subtilisin-related protease, TgSUB1, were reduced in Δ*crt* parasites. A) The abundance of secreted TgSUB1 in the constitutive and induced ESAs was measured by immunoblotting. There was no detectable TgSUB1 in the constitutive and induced ESAs secreted by Δ*crt* parasites via immunoblotting. **B)** The abundance of plasma membrane-anchored TgSUB1 was measured by staining non-permeabilized parasites with antibodies recognizing TgSUB1. The Δ*crt* mutant displayed a loss of TgSUB1 on its plasma membrane. **C)** TgSUB1 is a micronemal protein. TgSUB1 and TgMIC5 were both found to localize in the microneme in WT and Δ*crtCRT* parasites. However, TgSUB1 signal was not detected in the Δ*crt* parasites. **D)** The cell lysates of the Δ*crt* parasites showed that the steady level of TgSUB1 was reduced by ~90% in the Δ*crt* strain. **E)** The transcript levels of TgSUB1 were measured by quantitative PCR and were also decreased by approximately 90% in the Δ*crt* mutant. All assays listed in this figure were repeated at least in triplicate. Statistical significance was calculated using unpaired Student's *t*-test: ***, $p<0.001$; ****, $p<0.0001$; n.s., not significant.

Figure 5. The transcript and protein abundances of several VAC-residing proteases were decreased in Δ*crt*. A) RNA-Seq was performed in WT and Δ*crt* parasites. Each sample was sequenced in duplicate for statistical comparison. A volcano plot was used to display a summary of the genes that had altered transcription greater than 1.5-fold with statistical significance less than 0.05 in the Δ*crt* mutant relative to the WT strain. Forty-six and fifty-six genes labeled in blue and red dots became up- and down-regulated in the Δ*crt* mutant, respectively. The blue and red dash lines represented the border line of a 1.5-fold

transcriptional change of genes, and the genes above the black dash line showed *p* values of a statistical significance below 0.05. **B)** qPCR was used to validate 4 down-regulated proteases that were identified by RNA-Seq analysis, along with two known VAC proteases, TgCPL and TgCPB. *TgAMN*, *TgSCP*, *TgASP1*, and *TgCPB* displayed down-regulated transcription in Δ*crt* parasites compared to WT strain. **C)** The steady protein abundances of TgCPL and TgCPB were quantified in the lysates of parasites by immunoblotting. The protein levels of TgCPL and TgCPB in Δ*crt* mutant were reduced by ~25% and 60%, respectively, compared to WT parasites. **D)** TgSCP and TgAMN were endogenously tagged with 3xmyc and 3xHA, respectively, at their C-termini. The expression of the epitope-tagged proteins was confirmed by immunoblotting. The parasites were co-stained with antibodies recognizing their respective epitope tags as well as the VAC and ELC markers. Both TgSCP and TgAMN were localized in the VAC and ELC by immunofluorescence. Statistical significance was performed using unpaired Student's *t*-test. *, $p<0.05$; **, $p<0.01$; n.s., not significant.

Figure 6. Suppression of proteolysis in the VAC reduced VAC size and partially restored integrity of parasite's endolysosomal system, which recovered TgSUB1 expression, micronemal protein trimming in ESAs, and parasite invasion. A) The Δ*crt* parasites were incubated with 1 μM LHVS, an irreversible inhibitor of TgCPL, or with DMSO vehicle control, for 48 hrs, followed by a pulse invasion. Parasites were stained with anti-TgCPL antibodies to determine the size of the VAC. The swollen VAC phenotype was significantly reduced in the LHVS-treated parasites. Scale bar = 2μm. **B)** TgCPB, a VAC-residing endo- and exo-peptidase was genetically deleted in the Δ*crt* strain. A schematic illustration for the creation of the Δ*crt*Δ*cpb* mutant is shown. A PCR product carrying a pyrimethamine resistance cassette (DHFR) flanked by 50 bps of the 5'- and 3'-untranslated regions of *TgCPB* was transfected into WT parasites for double crossover replacement of *TgCPB*. Primers indicated in panel B were used to verify the replacement of *TgCPB* with *DHFR* via PCR and agarose gel electrophoresis. The ablation of *TgCPB* in Δ*crt*Δ*cpb* parasites was also confirmed by immunoblotting. **C)** The sizes of the VAC in WT, Δ*crt*, and Δ*crt*Δ*cpb* parasites were determined by the methods mentioned above. The Δ*crt*Δ*cpb* parasites displayed a partial reduction in the size of the VAC compared to WT parasites. **D)** Following pulse invasion, the

parasites were fixed, stained with anti-TgCPL (VAC marker) and proTgM2AP (ELC marker), and enumerated under immunofluorescence microscope. The parasites showing partial overlapping between the VAC and ELC in WT, Δ*crt*, Δ*crtCRT*, and Δ*crt*Δ*cpb* strains were quantified. At least 100 parasites were quantified for each replicate in a total of three replicates. The Δ*crt*Δ*cpb* parasites showed a significantly lower percentage of parasites having arrested co-localization between the VAC and ELC compared to the Δ*crt* mutant. **E)** The lysates of WT, Δ*crt*, and Δ*crt*Δ*cpb* parasites were probed with antibodies recognizing TgSUB1.The steady expression of TgSUB1 was restored in Δ*crt*Δ*cpb* parasites. **F)** The constitutive and induced ESAs of WT, Δ*crt*, and Δ*crt*Δ*cpb* strains were made and probed with the antibodies indicated in the figure. The secretion and trimming of micronemal proteins were also recovered in the Δ*crt*Δ*cpb* mutant. **G)** The invasion efficiencies of WT, Δ*crt*, and Δ*crt*Δ*cpb* strains were determined using the procedures mentioned above. The Δ*crt*Δ*cpb* parasites showed increased invasion efficiency compared to the Δ*crt* strain, albeit still a lower efficiency than that of WT parasites. Scale bar = 2 μm. Statistical significance was calculated using unpaired Student's *t*-test. *, $p<0.05$; ; **, $p<0.01$; ***, $p<0.001$; n.s., not significant.

Figure 7. A model for the regulation of the endolysosomal system in *Toxoplasma* parasites. *Toxoplasma* parasite contains a separate endosome-like compartment from the digestive vacuole within its endolysosomal system. When the parasite lacks TgCRT, the VAC becomes swollen and cannot separate from its adjacent ELC. This aberrant co-localization leads to reduced transcript and protein abundances of several proteases residing within the endolysosomal system, including TgSUB1. These changes alter the secretion of micronemal proteins, thereby resulting in invasion defects in the TgCRT-null mutant. ELC, endosome-like compartment; ER, endoplasmic reticulum; Go, Golgi apparatus; Mi, microneme; N, nucleus; Rh, rhoptry; TgCRT, *Toxoplasma* chloroquine resistance transporter ortholog; TgSUB1, *Toxoplasma* subtilisin 1; VAC, vacuolar compartment.

Table 1. Strains used in this study.

Name	Genetic background	Comments
WT	RH∆*ku80*∆*hxg*	Requested from the Carruthers Lab, not generated in this study
∆*crt*	RH∆*ku80*∆*hxg*∆*crt*	*TgCRT* was deleted by double crossover homologous recombination
∆*crtCRT*	RH∆*ku80*∆*hxg*∆*crt*::*TgCRT-mCherry-3xmyc*	Ectopic expression of a C-termially epitope-tagged TgCRT in ∆*crt* for complementation
∆*crt*∆*cpb*	RH∆ku80∆hxg∆*crt*∆*cpb*	The entire *TgCPB* gene was ablated by CRISPR-Cas9 based genome editing technique
WT::*nLuc*	RH∆*ku80*∆*hxg*::*nLuc*	Expressed NanoLuc luciferase in WT parasites
∆*crt*::*nLuc*	RH∆*ku80*∆*hxg*∆*crt*::*nLuc*	Expressed NanoLuc luciferase in ∆*crt* parasites
∆*crtCRT::nLuc*	RH∆*ku80*∆*hxg*∆*crt*::*TgCRT-mCherry-3xmyc::nLuc*	Expressed NanoLuc luciferase in ∆*crtCRT* parasites
TgAMN-3xHA	RH∆*ku80*∆*hxgTgAMN-3xHA*	*TgAMN* gene was endogenously tagged with a 3xHA epitope at its 3'-end by CRISPR-Cas9 based genome editing technique
TgSCP-3xmyc	RH∆*ku80*∆*hxgTgSCP-3xmyc*	*TgSCP* gene was endogenously tagged with a 3xmyc epitope at its 3'-end by single crossover recombination

Supplemental Figure Legends

S1 Figure. No defects in intramembrane proteolytic cleavage of micronemal protein 2 (TgMIC2) were observed in the ∆*crt* mutant. Purified, extracellular parasites that had not been permeabilized were stained with anti-TgMIC2 and anti-TgSAG1 antibodies in order to measure the retention of TgMIC2 on the parasite surface. During secretion, the TgMIC2 protein is cleaved by intramembrane rhomboid proteases, such as TgROM4. The abundance of TgMIC2 on the surface of ∆*crt* parasites was similar to that of the WT and ∆*crtCRT* strains, indicating that there is comparable intramembrane cleavage of TgMIC2 among the parasites with or without TgCRT. Scale bar = 2 µm.

S2 Figure. Schematic of the endogenous epitope-tagging of the *Toxoplasma* putative aminopeptidase N (TgAMN, TGGT1_221310) and the putative Pro-Xaa serine carboxypeptidase (TgSCP, TGGT1_254010). A) The plasmid encoding Cas9 and sgRNA targeting TgAMN were co-transfected into WT parasites with the PCR product carrying a 3xHA epitope tag and a pyrimethamine resistance cassette (DHFR) flanked by 50 bp regions upstream and downstream of the stop codon of TgAMN. The 3xHA tag and the drug resistance cassette were incorporated at the C-terminus of the

Toxoplasma putative aminopeptidase N via double crossover homologous recombination mediated by the CRISPR-Cas9 genome editing tool. **B)** The putative Pro-Xaa serine carboxypeptidase was endogenously tagged with a 3xmyc epitope tag at its C-terminus by single crossover homologous recombination. A 1 kb region upstream of the stop codon of TgSCP was amplified and fused at the 5'-end of the 3xmyc tag to produce the TgSCP-3xmyc tagged plasmid. The 1 kb TgSCP-coding region was cleaved by an endonuclease in the middle prior to transfection to facilitate its integration.

S3 Figure. The subcellular concave structure in the Δ*crt*Δ*cpb* mutant was reduced in size relative to the Δ*crt* strain during the extracellular stage. WT, Δ*crt*, Δ*crtCRT*, and Δ*crt*Δ*cpb* parasites were purified and attached on the surface of the slide for differential interference contrast (DIC) microscopy imaging. The Δ*crt*Δ*cpb* parasites still showed an enlarged concave subcellular structure (indicated by the arrow), however their sizes were significantly smaller than those in the Δ*crt* mutant. Scale bar = 5 μm.

S1 Table. Differential gene expression analysis between WT and *Δcrt* strains. The genes whose fold changes were >1.5 and *p*-values were <0.05 shown in RNA-Seq analysis were listed.

S2 Table. Primers used in this study.

References

1. Laliberté J, Carruthers VB. Host cell manipulation by the human pathogen *Toxoplasma gondii*. Cell Mol Life Sci. 2008;65: 1900–1915. doi:10.1007/s00018-008-7556-x

2. Carruthers VB, Tomley FM. Microneme proteins in apicomplexans. Subcell Biochem. 2008;47: 33–45.

3. Lagal V, Binder EM, Huynh M-H, Kafsack BFC, Harris PK, Diez R, et al. *Toxoplasma gondii* protease TgSUB1 is required for cell surface processing of micronemal adhesive complexes and efficient adhesion of tachyzoites. 2010;12: 1792–1808. doi:10.1111/j.1462-5822.2010.01509.x

4. Parussini F, Coppens I, Shah PP, Diamond SL, Carruthers VB. Cathepsin L occupies a vacuolar compartment and is a protein maturase within the endo/exocytic system of *Toxoplasma gondii*. Mol Microbiol. 2010;76: 1340–1357. doi:10.1111/j.1365-2958.2010.07181.x

5. Dogga SK, Mukherjee B, Jacot D, Kockmann T, Molino L, Hammoudi P-M, et al. A druggable secretory protein maturase of Toxoplasma essential for invasion and egress. Elife. 2017;6: 223. doi:10.7554/eLife.27480

6. Shen B, Buguliskis JS, Lee TD, Sibley LD. Functional analysis of rhomboid proteases during Toxoplasma invasion. MBio. 2014;5: e01795–14. doi:10.1128/mBio.01795-14

7. Buguliskis JS, Brossier F, Shuman J, Sibley LD. Rhomboid 4 (ROM4) affects the processing of surface adhesins and facilitates host cell invasion by *Toxoplasma gondii.* PLoS Pathog. 2010;6: e1000858. doi:10.1371/journal.ppat.1000858

8. Santos JM, Ferguson DJP, Blackman MJ, Soldati-Favre D. Intramembrane cleavage of AMA1 triggers *Toxoplasma* to switch from an invasive to a replicative mode. Science. 2011;331: 473–477. doi:10.1126/science.1199284

9. Parussini F, Tang Q, Moin SM, Mital J, Urban S, Ward GE. Intramembrane proteolysis of Toxoplasma apical membrane antigen 1 facilitates host-cell invasion but is dispensable for replication. Proc Natl Acad Sci USA. National Acad Sciences; 2012;109: 7463–7468. doi:10.1073/pnas.1114661109

10. Dou Z, Carruthers VB. Cathepsin proteases in *Toxoplasma gondii*. Adv Exp Med Biol. Boston, MA: Springer US; 2011;712: 49–61. doi:10.1007/978-1-4419-8414-2_4

11. Dou Z, McGovern OL, Di Cristina M, Carruthers VB. *Toxoplasma gondii* ingests and digests host cytosolic proteins. MBio. 2014;5: e01188–14. doi:10.1128/mBio.01188-14

12. Miller SA, Binder EM, Blackman MJ, Carruthers VB, Kim K. A conserved subtilisin-like protein TgSUB1 in microneme organelles of *Toxoplasma gondii*. J Biol Chem. 2001;276: 45341–45348. doi:10.1074/jbc.M106665200

13. Di Cristina M, Dou Z, Lunghi M, Kannan G, Huynh M-H, McGovern OL, et al. *Toxoplasma* depends on lysosomal consumption of autophagosomes for persistent infection. Nat Microbiol. 2017;2: 17096. doi:10.1038/nmicrobiol.2017.96

14. Dou Z, Coppens I, Carruthers VB. Non-canonical maturation of two papain-family proteases in *Toxoplasma gondii*. J Biol Chem. American Society for Biochemistry and Molecular Biology; 2013;288: 3523–3534. doi:10.1074/jbc.M112.443697

15. Warring SD, Dou Z, Carruthers VB, McFadden GI, van Dooren GG. Characterization of the chloroquine resistance transporter homologue in *Toxoplasma gondii*. Euk Cell. 2014;13: 1360–1370. doi:10.1128/EC.00027-14

16. Liu J, Pace D, Dou Z, King TP, Guidot D, Li Z-H, et al. A vacuolar-H^+-pyrophosphatase (TgVP1) is required for microneme secretion, host cell invasion, and extracellular survival of *Toxoplasma gondii*. Mol Microbiol. 2014;93: 698–712. doi:10.1111/mmi.12685

17. Juge N, Moriyama S, Miyaji T, Kawakami M, Iwai H, Fukui T, et al. *Plasmodium falciparum* chloroquine resistance transporter is a H^+-coupled polyspecific nutrient and drug exporter. Proc Natl Acad Sci USA. 2015;112: 3356–3361. doi:10.1073/pnas.1417102112

18. Huynh M-H, Carruthers VB. Tagging of endogenous genes in a *Toxoplasma gondii* strain lacking Ku80. Euk Cell. American Society for Microbiology; 2009;8: 530–539. doi:10.1128/EC.00358-08

19. Larson ET, Parussini F, Huynh M-H, Giebel JD, Kelley AM, Zhang L, et al. *Toxoplasma gondii* cathepsin L is the primary target of the invasion-inhibitory compound morpholinurea-leucyl-homophenyl-vinyl sulfone phenyl. J Biol Chem. 2009;284: 26839–26850. doi:10.1074/jbc.M109.003780

20. McGovern OL, Rivera-Cuevas Y, Kannan G, Narwold AJ, Carruthers VB. Intersection of endocytic and exocytic systems in *Toxoplasma gondii*. Traffic. Wiley/Blackwell (10.1111); 2018;19: 336–353. doi:10.1111/tra.12556

21. Blader IJ, Coleman BI, Chen C-T, Gubbels M-J. Lytic Cycle of Toxoplasma gondii: 15 Years Later. Annu Rev Microbiol. 2015;69: 463–485. doi:10.1146/annurev-micro-091014-104100

22. Dubremetz J-F. Rhoptries are major players in *Toxoplasma gondii* invasion and host cell interaction. Cell Microbiol. Wiley/Blackwell (10.1111); 2007;9: 841–848. doi:10.1111/j.1462-5822.2007.00909.x

23. Hager KM, Carruthers VB. MARveling at parasite invasion. Trends Parasitol. 2008;24: 51–54. doi:10.1016/j.pt.2007.10.008

24. Sloves P-J, Delhaye S, Mouveaux T, Werkmeister E, Slomianny C, Hovasse A, et al. Toxoplasma Sortilin-like Receptor Regulates Protein Transport and Is Essential for Apical Secretory Organelle Biogenesis and Host Infection. Cell Host Microbe. 2012;11: 515–527. doi:10.1016/j.chom.2012.03.006

25. Saouros S, Dou Z, Marchant J, Carruthers VB, Matthews S. Microneme protein 5 regulates the activity of *Toxoplasma* subtilisin 1 by mimicking a subtilisin prodomain. J Biol Chem. American Society for Biochemistry and Molecular Biology; 2012;287: 36029–36040. doi:10.1074/jbc.M112.389825

26. Binder EM, Lagal V, Kim K. The Prodomain of T*oxoplasma gondii* GPI-Anchored Subtilase TgSUB1 Mediates its Targeting to Micronemes. Traffic. 2008;9: 1485–1496. doi:10.1111/j.1600-0854.2008.00774.x

27. Settembre C, Di Malta C, Polito VA, Garcia Arencibia M, Vetrini F, Erdin S, et al. TFEB links autophagy to lysosomal biogenesis. Science. 2011;332: 1429–1433. doi:10.1126/science.1204592

28. Fu M, Blackshear PJ. RNA-binding proteins in immune regulation: a focus on CCCH zinc finger proteins. Nat Rev Immunol. 2017;17: 130–143. doi:10.1038/nri.2016.129

29. Carballo E, Lai WS, Blackshear PJ. Feedback Inhibition of Macrophage Tumor Necrosis Factor-α Production by Tristetraprolin. Science. American Association for the Advancement of Science; 1998;281: 1001–1005. doi:10.1126/science.281.5379.1001

30. Miranda K, Pace DA, Cintron R, Rodrigues JCF, Fang J, Smith A, et al. Characterization of a novel organelle in *Toxoplasma gondii* with similar composition and function to the plant vacuole. Mol Microbiol. 2010;76: 1358–1375. doi:10.1111/j.1365-2958.2010.07165.x

31. Warmka J, Hanneman J, Lee J, Amin D, Ota I. Ptc1, a type 2C Ser/Thr phosphatase, inactivates the HOG pathway by dephosphorylating the mitogen-activated protein kinase Hog1. Mol Cell Biol. 2001;21: 51–60. doi:10.1128/MCB.21.1.51-60.2001

32. Mapes J, Ota IM. Nbp2 targets the Ptc1-type 2C Ser/Thr phosphatase to the HOG MAPK pathway. EMBO J. 2004;23: 302–311. doi:10.1038/sj.emboj.7600036

33. González A, Ruiz A, Serrano R, Ariño J, Casamayor A. Transcriptional profiling of the protein phosphatase 2C family in yeast provides insights into the unique functional roles of Ptc1. J Biol Chem. 2006;281: 35057–35069. doi:10.1074/jbc.M607919200

34. Fidock DA, Nomura T, Talley AK, Cooper RA, Dzekunov SM, Ferdig MT, et al. Mutations in the *P. falciparum* Digestive Vacuole Transmembrane Protein PfCRT and Evidence for Their Role in Chloroquine Resistance. Mol Cell. Cell Press; 2000;6: 861–871. doi:10.1016/S1097-2765(05)00077-8

35. Lewis IA, Wacker M, Olszewski KL, Cobbold SA, Baska KS, Tan A, et al. Metabolic QTL analysis links chloroquine resistance in *Plasmodium falciparum* to impaired hemoglobin catabolism. Neafsey DE, editor. PLoS Genet. 2014;10: e1004085. doi:10.1371/journal.pgen.1004085

36. Shen B, Brown KM, Lee TD, Sibley LD. Efficient Gene Disruption in Diverse Strains of Toxoplasma gondii Using CRISPR/CAS9. MBio. 2014;5: e01114–14–e01114–14. doi:10.1128/mBio.01114-14

37. Sidik SM, Hackett CG, Tran F, Westwood NJ, Lourido S. Efficient Genome Engineering of Toxoplasma gondii Using CRISPR/Cas9. Blader IJ, editor. PLoS ONE. 2014;9: e100450–8. doi:10.1371/journal.pone.0100450

38. Kaja S, Payne AJ, Singh T, Ghuman JK, Sieck EG, Koulen P. An optimized lactate dehydrogenase release assay for screening of drug candidates in neuroscience. Journal of Pharmacological and Toxicological Methods. 2015;73: 1–6. doi:10.1016/j.vascn.2015.02.001

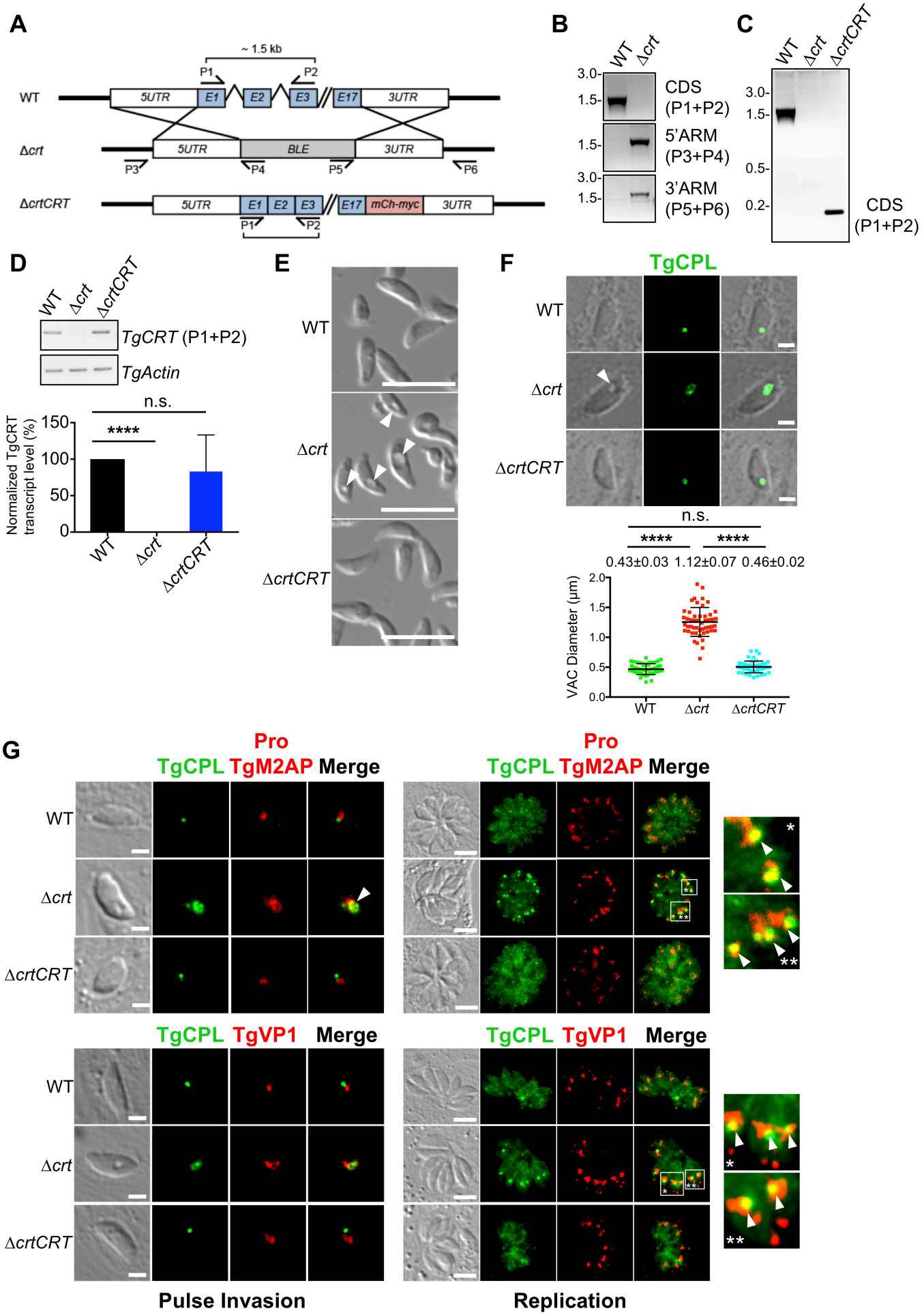
A
~ 1.5 kb
P1
P2
WT
5UTR
E1
E2
E3
E17
3UTR
Δcrt
BLE
P3
P4
P5
P6
ΔcrtCRT
mCh-myc
B
WT
Δcrt
3.0-
1.5-
CDS (P1+P2)
5'ARM (P3+P4)
3'ARM (P5+P6)
C
0.5-
0.2-
CDS (P1+P2)
D
TgCRT (P1+P2)
TgActin
n.s.
****
Normalized TgCRT transcript level (%)
150
100
50
0
E
F
TgCPL
0.43±0.03
1.12±0.07
0.46±0.02
VAC Diameter (µm)
2.0
1.5
1.0
0.5
0.0
G
Pro
TgCPL TgM2AP Merge
TgCPL TgVP1 Merge
Pulse Invasion
Replication

Figure 1

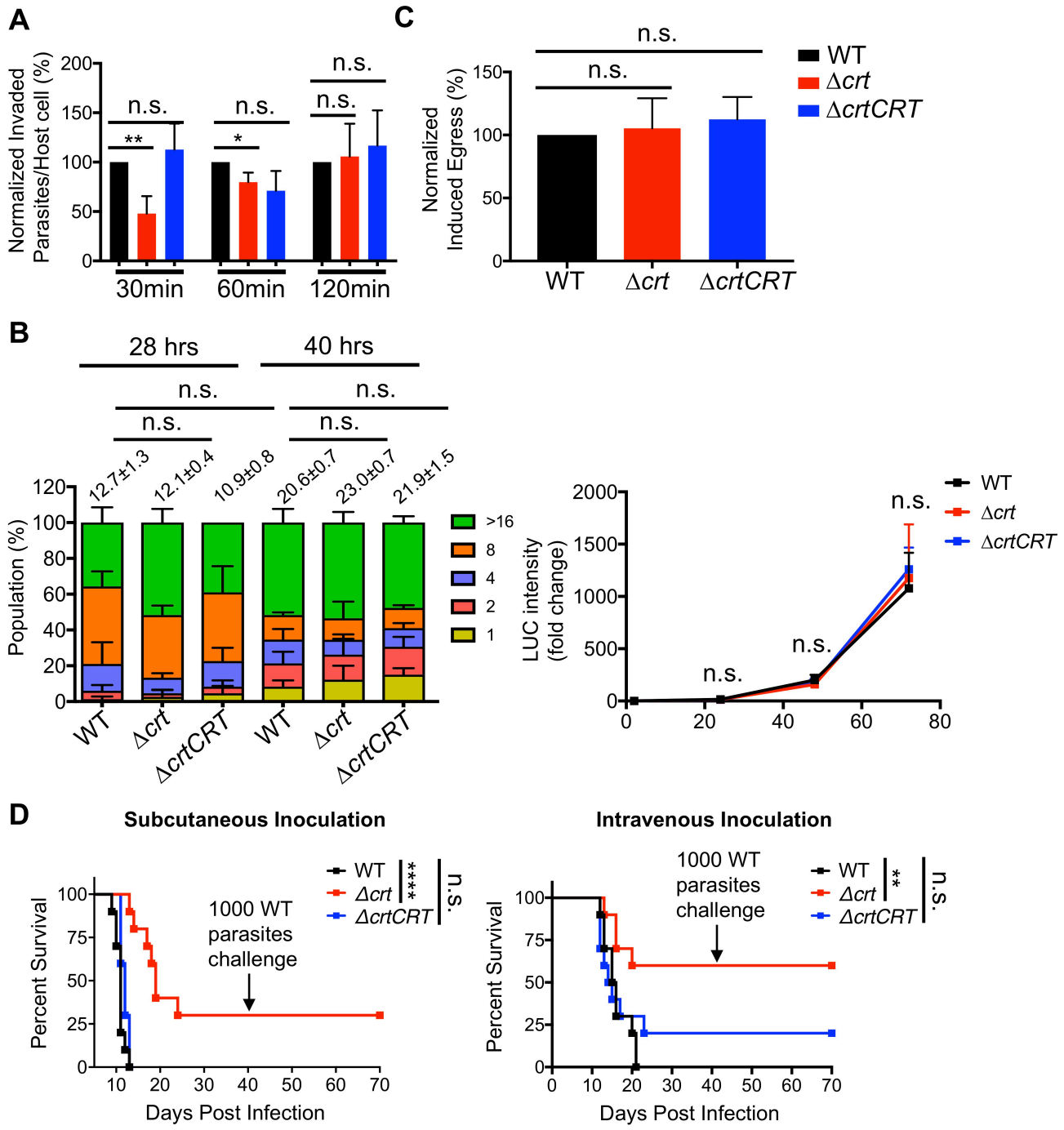
A
Normalized Invaded Parasites/Host cell (%)
200
150
100
50
0
n.s.
**
n.s.
*
n.s.
n.s.
30min
60min
120min
C
Normalized Induced Egress (%)
150
100
50
0
n.s.
n.s.
WT
Δcrt
ΔcrtCRT
B
28 hrs
40 hrs
n.s.
n.s.
n.s.
n.s.
12.7±1.3
12.1±0.4
10.9±0.8
20.6±0.7
23.0±0.7
21.9±1.5
Population (%)
120
100
80
60
40
20
0
>16
8
4
2
1
LUC intensity (fold change)
2000
1500
1000
500
0
n.s.
n.s.
n.s.
0
20
40
60
80
D
Subcutaneous Inoculation
Intravenous Inoculation
Percent Survival
1000 WT parasites challenge
****
n.s.
**
n.s.
Days Post Infection

Figure 2

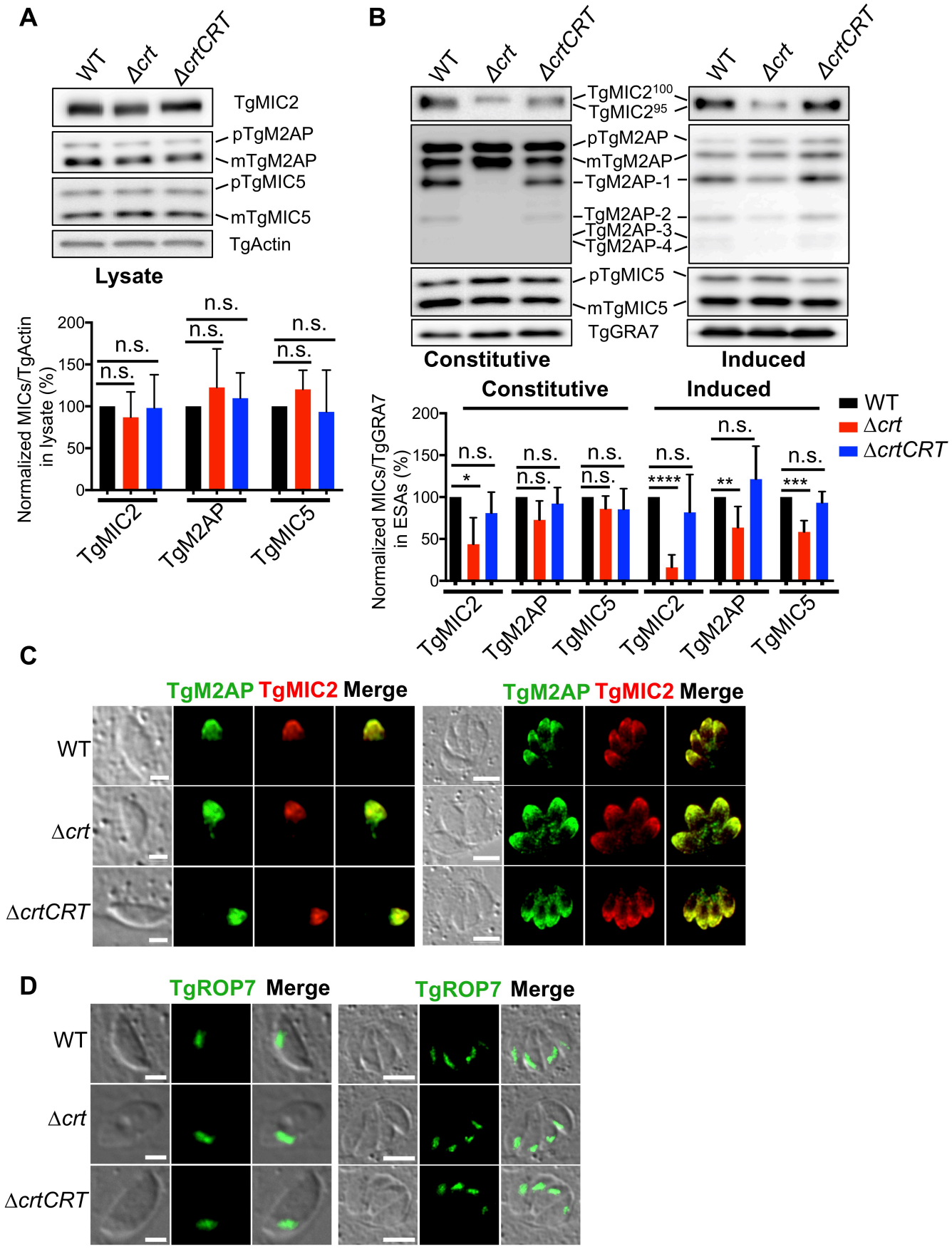
A
WT
Δcrt
ΔcrtCRT
TgMIC2
pTgM2AP
mTgM2AP
pTgMIC5
mTgMIC5
TgActin
Lysate
Normalized MICs/TgActin in lysate (%)
200
150
100
50
0
n.s.
TgMIC2
TgM2AP
TgMIC5
B
TgMIC2100
TgMIC295
TgM2AP-1
TgM2AP-2
TgM2AP-3
TgM2AP-4
TgGRA7
Constitutive
Induced
Normalized MICs/TgGRA7 in ESAs (%)
*
****
**
***
WT
Δcrt
ΔcrtCRT
C
TgM2AP TgMIC2 Merge
D
TgROP7 Merge

Figure 3

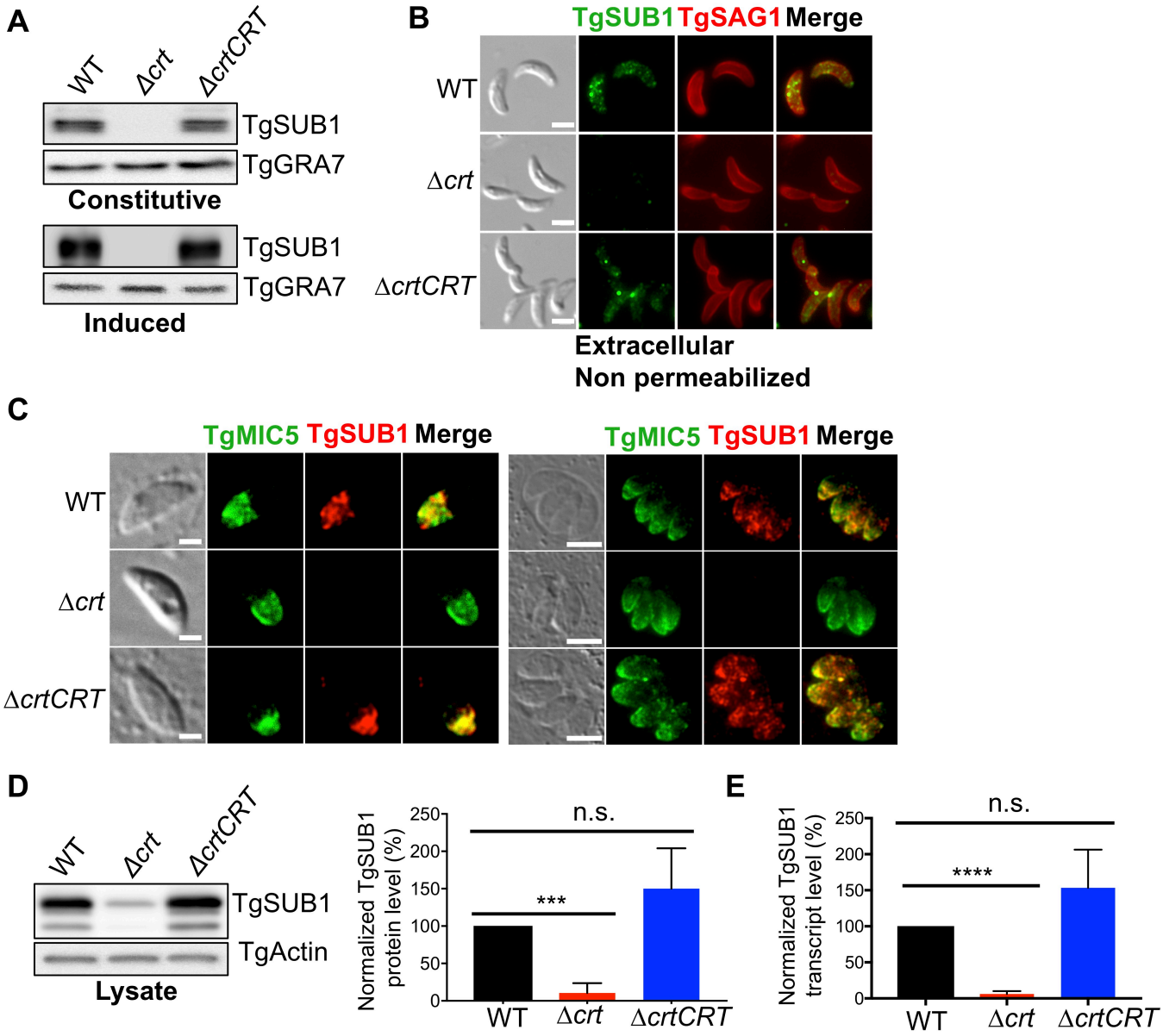
A
WT
Δcrt
ΔcrtCRT
TgSUB1
TgGRA7
Constitutive
TgSUB1
TgGRA7
Induced
B
TgSUB1 TgSAG1 Merge
WT
Δcrt
ΔcrtCRT
Extracellular
Non permeabilized
C
TgMIC5 TgSUB1 Merge
TgMIC5 TgSUB1 Merge
WT
Δcrt
ΔcrtCRT
D
WT
Δcrt
ΔcrtCRT
TgSUB1
TgActin
Lysate
Normalized TgSUB1 protein level (%)
250
200
150
100
50
0
n.s.
***
WT
Δcrt
ΔcrtCRT
E
Normalized TgSUB1 transcript level (%)
250
200
150
100
50
0
n.s.
****
WT
Δcrt
ΔcrtCRT

Figure 4

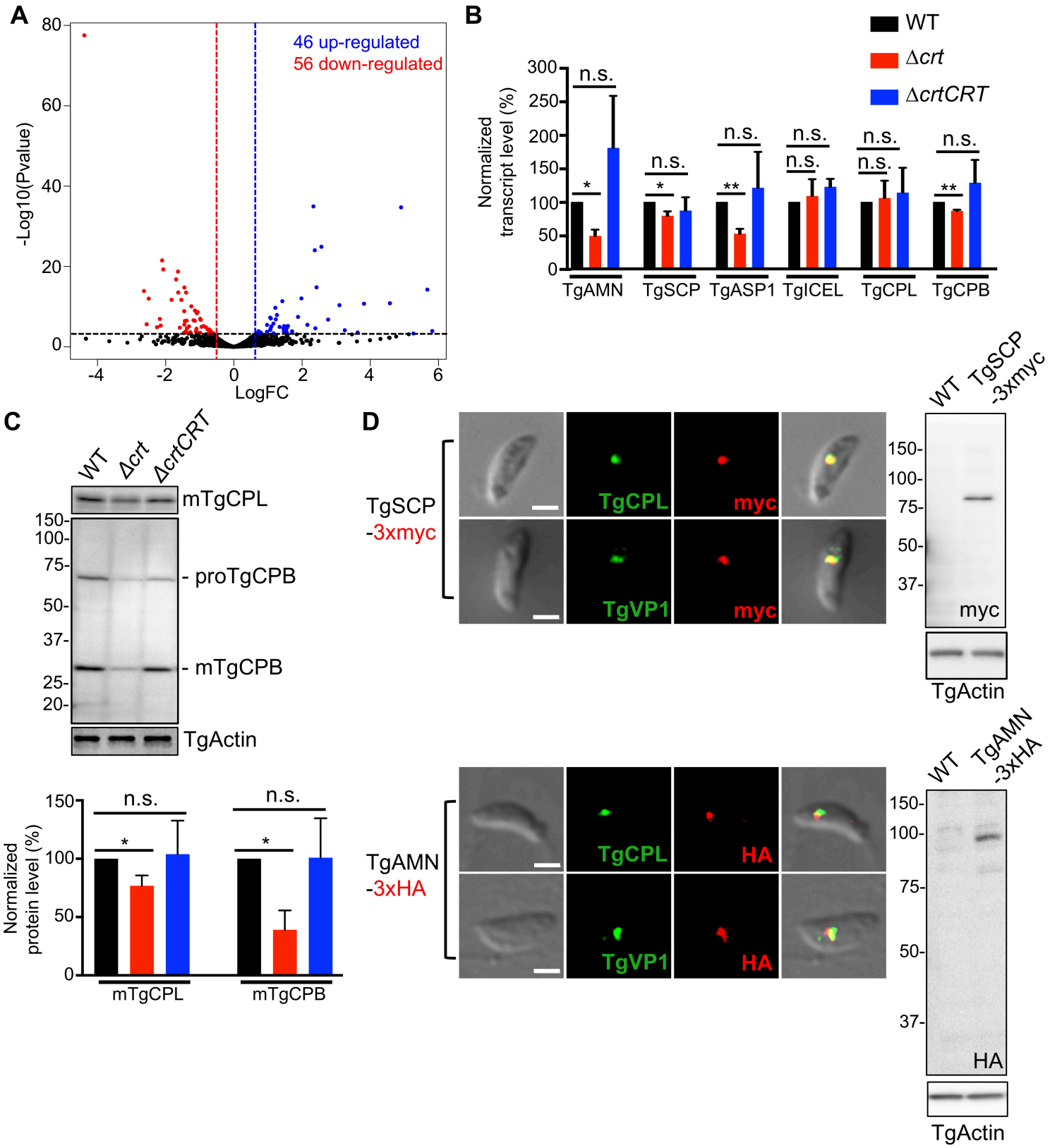
A
46 up-regulated
56 down-regulated
-Log10(Pvalue)
LogFC
B
WT
Δcrt
ΔcrtCRT
Normalized transcript level (%)
n.s.
*
**
TgAMN
TgSCP
TgASP1
TgICEL
TgCPL
TgCPB
C
WT
Δcrt
ΔcrtCRT
mTgCPL
- proTgCPB
- mTgCPB
TgActin
Normalized protein level (%)
mTgCPL
mTgCPB
D
TgSCP -3xmyc
TgCPL
myc
TgVP1
WT
TgSCP -3xmyc
TgAMN -3xHA
HA
TgActin

Figure 5

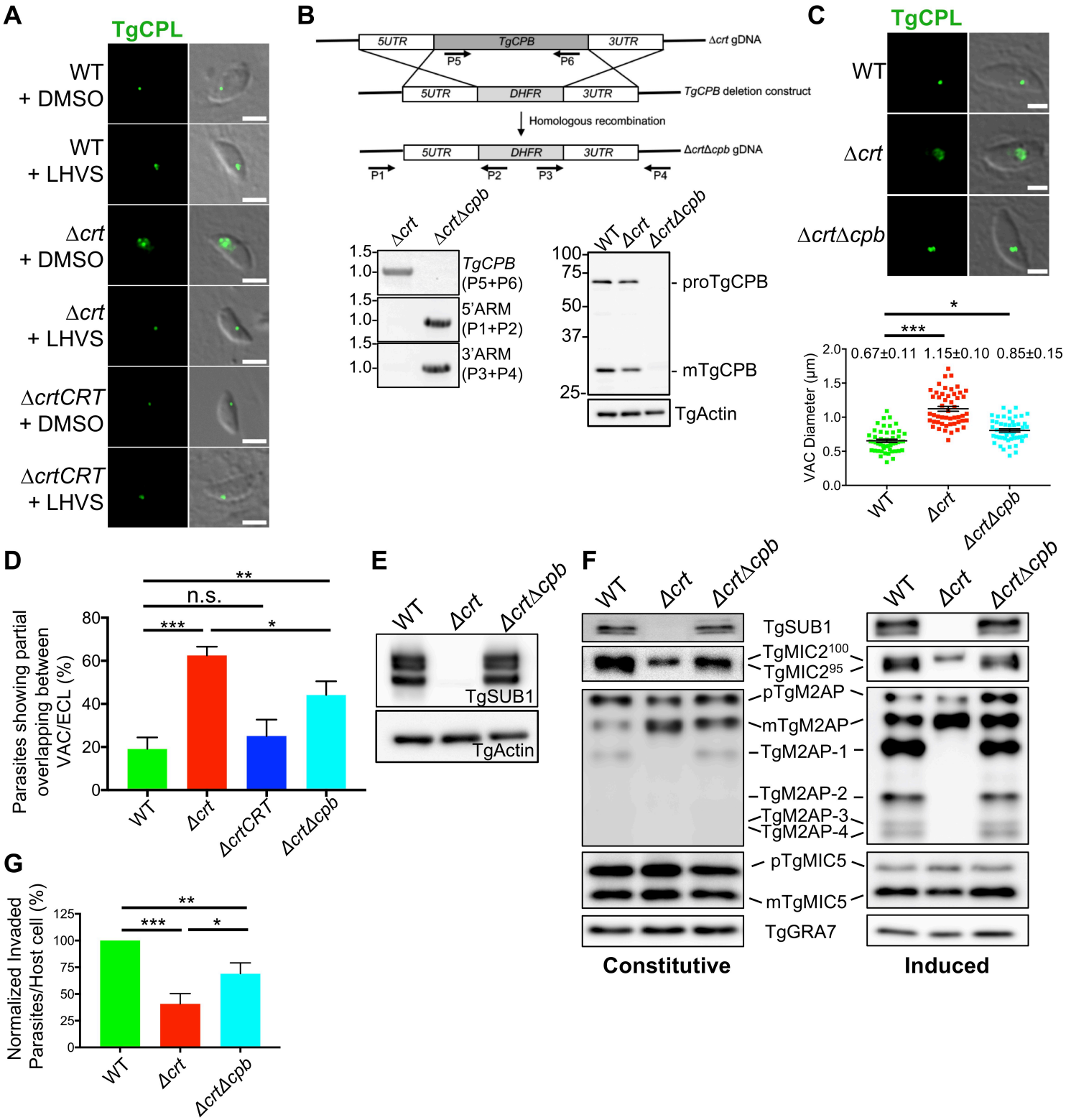
A
TgCPL
WT + DMSO
WT + LHVS
Δcrt + DMSO
Δcrt + LHVS
ΔcrtCRT + DMSO
ΔcrtCRT + LHVS
B
5UTR
TgCPB
3UTR
Δcrt gDNA
P5
P6
5UTR
DHFR
3UTR
TgCPB deletion construct
Homologous recombination
5UTR
DHFR
3UTR
ΔcrtΔcpb gDNA
P1
P2
P3
P4
Δcrt
ΔcrtΔcpb
TgCPB (P5+P6)
5'ARM (P1+P2)
3'ARM (P3+P4)
WT
Δcrt
ΔcrtΔcpb
proTgCPB
mTgCPB
TgActin
C
TgCPL
WT
Δcrt
ΔcrtΔcpb
VAC Diameter (μm)
0.67±0.11
1.15±0.10
0.85±0.15
D
Parasites showing partial overlapping between VAC/ECL (%)
n.s.
WT
Δcrt
ΔcrtCRT
ΔcrtΔcpb
E
WT
Δcrt
ΔcrtΔcpb
TgSUB1
TgActin
F
WT
Δcrt
ΔcrtΔcpb
TgSUB1
TgMIC2100
TgMIC2 95
pTgM2AP
mTgM2AP
TgM2AP-1
TgM2AP-2
TgM2AP-3
TgM2AP-4
pTgMIC5
mTgMIC5
TgGRA7
Constitutive
Induced
G
Normalized Invaded Parasites/Host cell (%)
WT
Δcrt
ΔcrtΔcpb

Figure 6

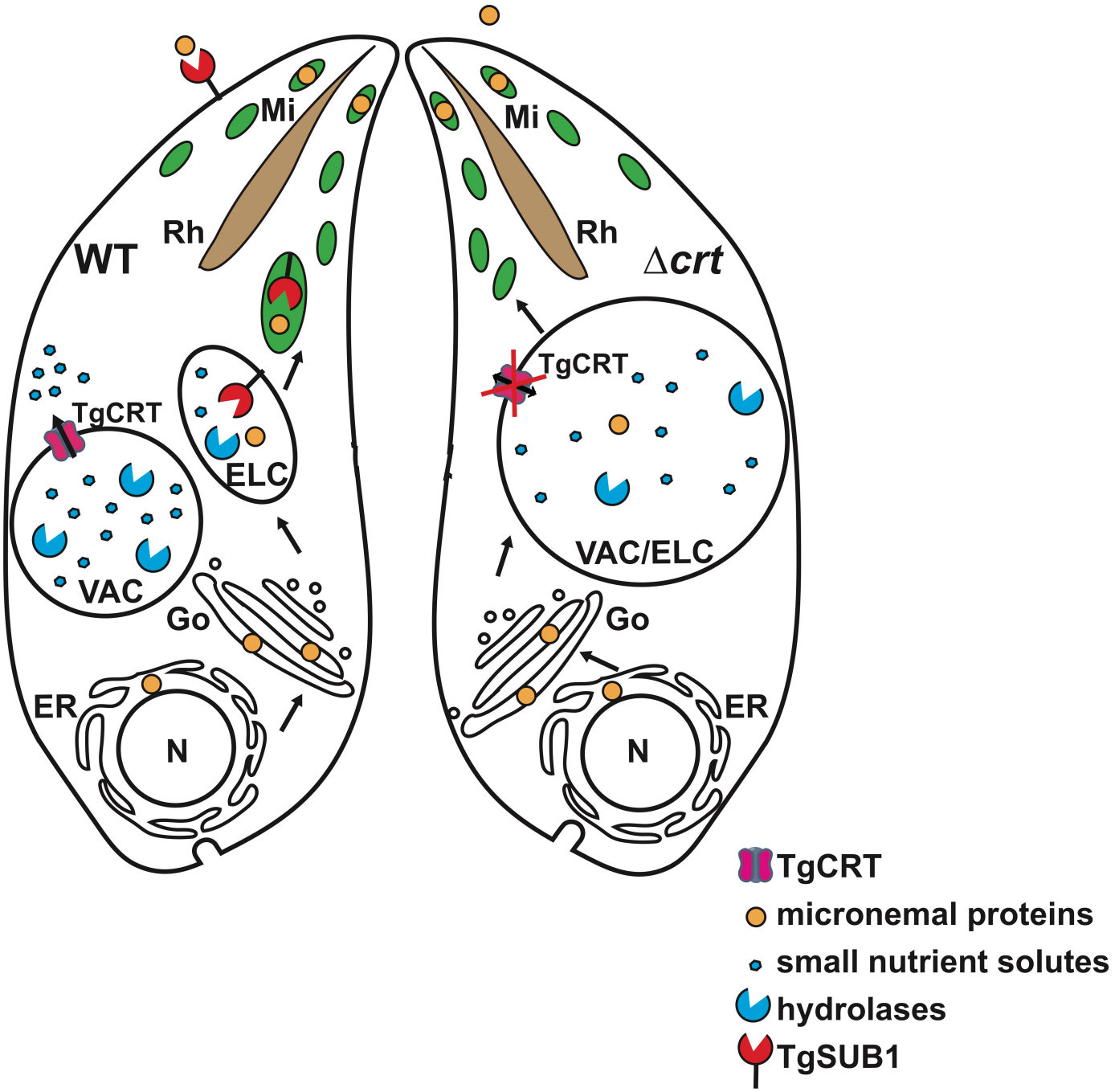
WT
Mi
Rh
TgCRT
ELC
VAC
Go
ER
N
Δcrt
Mi
Rh
TgCRT
VAC/ELC
Go
ER
N
TgCRT
micronemal proteins
small nutrient solutes
hydrolases
TgSUB1

Figure 7